JBC Papers in Press. Published on September 12, 2017 as Manuscript M117.811489
The latest version is at http://www.jbc.org/cgi/doi/10.1074/jbc.M117.811489

Multiple mechanisms contribute to increased neutral lipid accumulation in yeast producing recombinant variants of plant diacylglycerol acyltransferase 1

Yang Xu[1], Guanqun Chen[1], Michael S. Greer[1], Kristian Mark. P. Caldo[1,2], Geetha Ramakrishnan[1], Saleh Shah[1], Limin Wu[3], M. Joanne Lemieux[2], Jocelyn Ozga[1], and Randall J. Weselake[1*]

[1]Department of Agricultural, Food and Nutritional Science, University of Alberta, Edmonton, Alberta, Canada T6G 2P5

[2]Department of Biochemistry, University of Alberta, Edmonton, Alberta, Canada T6G 2H7

[3]Crop Pathology and Biotechnology, InnoTech Alberta, Vegreville, Alberta, Canada T9C 1T4

Running title: Plant DGAT1 variants with enhanced performance

[*] To whom correspondence should be addressed: Randall J. Weselake, Department of Agricultural, Food and Nutritional Science, University of Alberta, Edmonton, Alberta, Canada T6G 2P5, Phone: (+1) 306 261-0560; E-mail: randall.weselake@ualberta.ca

Key words: triacylglycerol biosynthesis; DGAT; substrate inhibition; oilseed rape; *Brassica napus*; *Camelina sativa*; *Saccharomyces cerevisiae*

Abstract

The apparent bottleneck in the accumulation of oil during seed development in some oleaginous plant species is the formation of triacylglycerol (TAG) by the acyl-CoA-dependent acylation of *sn*-1,2-diacylglycerol catalyzed by diacylglycerol acyltransferase (DGAT, EC 2.3.1.20). Improving DGAT activity using protein engineering could lead to improvements in seed oil yield, for example in canola-type *Brassica napus*. Directed evolution of *B. napus* DGAT1 (BnaDGAT1) previously revealed that one of the regions where amino acid residue substitutions leading to higher performance in BnaDGAT1 was in the ninth predicted transmembrane domain (PTMD9). In this study, several BnaDGAT1 variants with amino acid residue substitutions in PTMD9 were characterized. Among these enzyme variants, the extent of yeast TAG production was affected by different mechanisms including increased enzyme activity, increased polypeptide accumulation and possibly reduced substrate inhibition. The kinetic properties of the BnaDGAT1 variants were affected by the amino acid residue substitutions and a new kinetic model based on substrate inhibition and sigmoidicity was generated. Based on sequence alignment and further biochemical analysis, the amino acid residue substitutions that conferred increased TAG accumulation were

shown to be present in the DGAT1-PTMD9 region of other higher plant species. When amino acid residue substitutions that increased BnaDGAT1 enzyme activity were introduced into recombinant *Camelina sativa* DGAT1, they also improved enzyme performance. Thus, the knowledge generated from directed evolution of DGAT1 in one plant species can be transferred to other plant species and has potentially broad applications in genetic engineering of oleaginous crops and microorganisms.

Canola-type *Brassica napus* is Canada's major oilseed crop. In 2016, canola seed production was about 18.4 million tonnes, contributing $26.7 billion in economic activity (Canola Council of Canada, http://www.canolacouncil.org/). A one percent absolute increase in canola seed oil content could potentially result in an additional $90 million per year for the seed oil extraction and processing industry in Canada (Canola Council of Canada). Triacylglycerol (TAG) is the predominant component of seed oil which is mainly used for food (1). In addition, seed TAG is used in the production of biodiesel, cosmetics, surfactants, lubricants, and paints (2). The development of strategies to increase seed oil content can benefit from a deeper understanding of TAG biosynthetic pathways.

During seed development, TAG is synthesized via acyl-CoA-dependent or acyl-CoA-independent pathways (3). Diacylglycerol acyltransferase (DGAT, EC 2.3.1.20) catalyzes the acyl-CoA-dependent acylation of *sn*-1,2-diacylglycerol to produce TAG and CoA (4). Two forms of membrane-bound DGAT (DGAT1 and DGAT2), which essentially share no amino acid sequence homology, have been identified in eukaryotes (5). In some oilseed species, the level of DGAT activity during seed development appears to have a substantial effect on the flow of carbon into seed TAG (6). Over-expression of *DGAT1* during seed development leads to increased seed oil content in *B. napus* (7, 8), soybean (*Glycine max*) (9, 10), maize (*Zea mays*) (11) and Arabidopsis (*Arabidopsis thaliana*) (12). Further increase in seed oil content might be achieved by the introduction of DGAT modified through protein engineering.

DGAT, however, contains multiple transmembrane domains (TMDs), and to date, there is no three-dimensional structure available for any DGAT (13, 14). Directed evolution is a powerful approach to increase enzyme activity especially in the absence of a three-dimensional protein structure. In addition, directed evolution together with site directed mutagenesis has been useful in gaining insights into enzyme structure-function relationships (15, 16). Previously, we used directed evolution to successfully generate numerous *B. napus* DGAT1 (BnaDGAT1, Genbank accession No.: JN224473) variants resulting in increased TAG accumulation in *Saccharomyces cerevisiae* strain H1246 (*MATα are1-Δ::HIS3, are2-Δ::LEU2, dga1-Δ::KanMX4, lro1-Δ::TRP1 ADE2*, designated 4 delta) (4). Further analysis revealed that the ninth predicted

TMD (PTMD9) contains key amino acid residue substitutions leading to higher performance in BnaDGAT1. Two variants (L441P and I447F) with amino acid residue substitutions in that region have been found to increase oil content when the encoding cDNAs were expressed in yeast and *Nicotiana benthamiana* leaves (17). Despite this, little is known about how these amino acid residue substitutions affect DGAT1 performance. A number of questions can be posed in this regard. Is the observed increase in oil content attributable to the increased enzyme activity, increased polypeptide accumulation or both? Are the specific amino acid residue substitutions associated with the changes in the kinetic properties of the enzyme? Since the BnaDGAT1-PTMD9 is moderately conserved among various DGAT1, does this domain contain key amino acid residues influencing DGAT1 activity in a range of oleaginous plant species? Finally, could the beneficial amino acid residue substitutions identified in BnaDGAT1-PTMD9 be used to guide the modification of another plant DGAT1?

To answer these questions, three BnaDGAT1 variants (L441P, I447F and F449C) with amino acid residue substitutions in PTMD9 and one out-group variant, V125F, were chosen for characterization. These recombinant variants were characterized as having higher enzyme activity and/or exhibiting increased polypeptide accumulation in the yeast system. Possible reduced substrate inhibition also appeared to contribute to increased oil content in yeast. Sequence alignment of DGAT1 revealed that the PTMD9 is conserved in many plant species. When the amino acid residue substitutions that led to increased enzyme performance were introduced into a recombinant *Camelina sativa* DGAT1 (CsDGAT1B, Genbank accession No.: XM_010417066), the performance of CsDGAT1B was improved.

Results

BnaDGAT1 variants increased yeast neutral lipid content through increased activity and/or polypeptide accumulation

Previously, directed evolution of BnaDGAT1 generated numerous variants resulting in increased TAG accumulation in yeast strain 4 delta (4, 18). To investigate the underlying mechanisms responsible for the increased neutral lipid content, several BnaDGAT1 variants were assessed for *in vitro* enzyme activity and protein production level. The relative levels of DGAT activity and protein accumulation varied among the variants (Fig. S1A). When compared to the wild type (WT) BnaDGAT1, the majority of the enzyme variants displayed higher activity, increased polypeptide accumulation, or higher activity combined with increased polypeptide accumulation (Fig. S1A). Interestingly, some BnaDGAT1 variants resulted in decreased *in vitro* enzyme activity and/or decreased polypeptide accumulation even though the introduction of these variants resulted in increased TAG accumulation in yeast compared to WT BnaDGAT1 (Fig. S1A). This might be explained by the dynamic changes in enzyme

activity of BnaDGAT1 variants in yeast over their growth phase (Fig. S1B). Based on these initial results (Fig. S1), it was hypothesized that the increased TAG production (as reflected by increased neutral lipid production) in yeast is due to increased enzyme activity, increased polypeptide accumulation or a combination of enzyme activation and increased polypeptide accumulation. To test this hypothesis, six BnaDGAT1 variants with widely distributed amino acid residue substitutions throughout the entire polypeptide were chosen from our previously established directed evolution library for characterization. Neutral lipid content in yeast cultures producing these variants was confirmed to be equal to or higher than yeast producing the recombinant WT enzyme by the Nile red assay (Fig. 1A). Since the enzyme activities and protein accumulation of the BnaDGAT1 polypeptide varied during yeast growth, their production profiles were examined. The production of the variant enzymes followed a similar pattern after induction. The activity of the recombinant enzymes increased markedly during the log phase, and then decreased after reaching the stationary phase (Fig. 1B). The highest activity of each variant occurred at the late log or early stationary phase. Significant increases in DGAT activity were observed for all variants relative to that of the WT enzyme except for K289N, which displayed relative activities over time similar to the WT enzyme (Fig. 1C). The microsomes displaying the highest activity of each variant were analyzed for their corresponding recombinant protein accumulation (Fig. 1D). When compared with recombinant WT BnaDGAT1, all recombinant BnaDGAT1 variants exhibited equal or higher band density with the exception of K289N. The enzyme activities were then normalized to the Western blot results and the normalized relative activity of each variant was similar to or higher than that of the WT enzyme (Fig. 1E).

Impact of amino acid substitutions in the 9th predicted transmembrane domain on enzyme activity and accumulation in yeast

In a previous study, directed evolution of BnaDGAT1 revealed that PTMD9 contains important amino acid residue substitutions affecting DGAT1 performance (17). In order to further investigate the effects of mutations in PTMD9 on enzyme activity and accumulation in yeast, three variants including L441P, I447F and F449C with amino acid residue substitutions in BnaDGAT1-PTMD9 were characterized in detail. Similar to previous results, variant L441P or I447F displayed increased enzyme activity relative to that of the WT enzyme (Fig. S2). It is interesting to note that L441P, I447F or F449C had very different effects on enzyme activity (Fig. 1B and S2) and accumulation (Fig. 2A and 2B) even though all amino acid residue substitutions are located very closely in PTMD9 of BnaDGAT1. The normalized relative activity of L441P or F449C was significantly higher than that of WT BnaDGAT1. I447F, however, displayed comparable normalized activity to WT enzyme (Fig. 2C).

Altered polypeptide accumulation levels for the recombinant BnaDGAT1 variants in yeast 4 delta, however, might be attributable to variations in cDNA expression. DNA copy number and expression level of each *BnaDGAT1* variant were assessed by qPCR. All plasmids containing *BnaDGAT1* and its variants showed similar copy number (Fig. S3A). Consistent with previous results (17), *BnaDGAT1* and its variants displayed high expression levels in the yeasts (Fig. S3B) and no significant difference was observed for the selected *BnaDGAT1* variants compared to that of WT *DGAT1*.

Kinetic characterization of microsomal recombinant BnaDGAT1 variants

To kinetically characterize the effects of the single amino acid residue substitutions in BnaDGAT1-PTMD9, the activities of microsomal recombinant BnaDGAT1 variants (L441P, I447F, F449C and the out-group variant V125F) were examined over a range of oleoyl-CoA concentrations (Fig. 3), which were below the critical micelle concentration of oleoyl-CoA (about 30 μM) (19). Variant V125F, I447F or F449C exhibited a similar enzyme activity dependence on increasing acyl donor concentration to microsomes containing the recombinant WT BnaDGAT1. DGAT1 activity increased markedly at low oleoyl-CoA concentration ranging from 0.1 to 5 μM and then the enzyme activity reduced gradually with further increases in oleoyl-CoA concentration. Variant L441P, however, displayed high activity at all oleoyl-CoA concentrations examined, suggesting that this enzyme variant may have a better tolerance for increased oleoyl-CoA concentration.

The initial reaction velocity data of BnaDGAT1 and its variants were fitted to the Michaelis-Menten or substrate inhibition equation, and the substrate inhibition kinetics was the preferred model for all these BnaDGAT1 variants (Fig. 3A-E). The apparent kinetic parameters were calculated and are summarized in Table 1. Kinetic parameters are indicated as being 'apparent' because the enzyme, acyl acceptor (*sn*-1,2-diacylglycerol) and triacylglycerol product are all insoluble contributing to a potentially complex kinetic situation. Variant L441P displayed weak substrate inhibition for oleoyl-CoA, with K_i^{app} value increasing as much as 6.4-fold, compared with the WT BnaDGAT1 value of about 13.9 μM. There was also a slight increase (1.3 fold) of variant F449C, whereas no change in the K_i^{app} value for I447F or V125F was observed. Most microsomal recombinant BnaDGAT1 variants exhibited greater V_{max}^{app} values than the microsomal recombinant WT enzyme. After adjusting for protein abundance, the $V_{max}{}'^{app}$ values of the microsomal recombinant BnaDGAT1 variants ranged from about 1.2 to 2.4-fold greater than that of the WT BnaDGAT1 value of 6.09 nmol/min/mg microsomal protein. K_m^{app} values for the BnaDGAT1 variants were slightly higher than that of WT BnaDGAT1 with the exception of L441P. The catalytic efficiencies ($V_{max}{}'^{app} / K_m^{app}$) of variant L441P and V125F were improved to 162% and 184%, respectively, over WT BnaDGAT1.

The N-terminal fragments of *Bna*A.DGAT1.b (GenBank ID: AF164434.1), another DGAT1 isoform from *B. napus*, and mouse DGAT1 (20) were shown to bind acyl-CoA in a cooperative manner (21). Recently, it has been reported that DGAT1s from *C. americana* and maize displayed sigmoidal kinetics in response to increasing acyl-CoA at lower concentration (10). A closer look at the initial reaction velocities at lower oleoyl-CoA concentration (Fig. 3F-J) showed that microsomal recombinant WT BnaDGAT1 and its variants in fact exhibited sigmoidal kinetics.

Sequence alignment of the 9th predicted transmembrane domain of BnaDGAT1 among various DGAT1s

Given the fact that amino acid residue substitutions in BnaDGAT1-PTMD9 improved enzyme performance, it was hypothesized that PTMD9 would also be present in other DGAT1s. Amino acid sequence alignment of 43 DGAT1s suggested that PTMD9 of BnaDGAT1 is moderately conserved, with 59.6% sequence identity among all species and 79.2% sequence identity among DGAT1s from the plant kingdom (Fig. 4). Different conservation levels were observed for the beneficial amino acid residue substitutions in BnaDGAT1-PTMD9, including L441P, I447F and F449C. According to the phylogenetic tree, BnaDGAT1-L441 and I447 are highly conserved among the DGAT1 from order *Rosids* and land plants, respectively, whereas BnaDGAT1-F449 is more divergent. The high conservation of the beneficial amino acid residues in the predicted TMD9 suggested the possibility of modifying DGAT1 from other species by using the information obtained from BnaDGAT1.

Creation of high performance Camelina sativa DGAT1 variants

It was hypothesized that the amino acid residue substitutions resulting in the improved performance of BnaDGAT1 could be installed in DGAT1 enzymes for other oil crops. *C. sativa* is an emerging oil crop, which possesses important agronomic traits and is considered as an ideal platform for the production of oil feedstock for biofuels and industrial compounds (22). Three *C. sativa DGAT1* (*CsDGAT1A, B, C*) cDNAs were identified from developing *C. sativa* (cv. CAME) seeds (23). The deduced amino acid sequences of the three *CsDGAT1* genes shared 98.5% sequence identity and around 85% sequence identity when compared with BnaDGAT1 (Fig. S4). To determine whether the benefical amino acid residue substitutions in BnaDGAT1-PTMD9 also could improve a DGAT1 from another species, the corresponding substituitons of two conserved BnaDGAT1 variants (L441P and I447F) in BnaDGAT1-PTMD9 and one out-group variant V125F (in the first predicted TMD) were introduced into CsDGAT1B (I144F, L460P and I466F, Fig. S4). As shown in Fig. 5A, the three single CsDGAT1B variants (I144F, L460P and I466F) and a double mutant L460P/I466F were produced in yeast 4 delat to determine the effects on neutral lipid content. The introduction of all four recombinant CsDGAT1B variants resulted in increased neutral lipid accumulation when

compared to the effect of recombinant WT CsDGAT1B.

Microsomal fractions containing recombinant CsDGAT1 variants were prepared from corresponding yeast cultures harvested with similar optical density values at 600 nm (OD_{600}, about 7.5) at mid log phase and were used to determine enzyme activity. All of the variants exhibited higher DGAT activity than the WT enzyme, increasing as much as 6-fold for the most effective CsDGAT1B variants L460P and L460P/I466F (Fig. 5B). Substrate inhibition kinetics were also observed for microsomal recombinant CsDGAT1B and the variants of CsDGAT1B (Fig. 5C). The apparent kinetic parameters were calculated based on the substrate inhibition equation (Table 2). The kinetics of microsomal CsDGAT1B variants were similar to what was observed using yeast microsomes containing the corresponding recombinant BnaDGAT1 variants. All of the CsDGAT1B variants had greater V_{max}^{app} values (ranging from about 3.6 to 8.3-fold) than the V_{max}^{app} of 0.09 nmol/min/mg microsomal protein determined for the recombinant WT enzyme. V_{max}^{app} could not be adjusted by protein abundance as the V5 tag was not included in the CsDGAT1B variants. K_m^{app} values of the variants were slightly higher than that of WT CsDGAT1B, with the exception of L460P and L460P/I466F. CsDGAT1B variant L460P displayed weak substrate inhibition for oleoyl-CoA, with K_i^{app} value increasing as much as about 6.7-fold compared to the WT CsDGAT1B value of 7.22 μM. For the double mutant L460P/I466F, a 1.6-fold increase in K_i^{app} values was observed. However, I144F had a decreased K_i^{app} value (2.88 μM). A sigmoidal response of enzyme activity to increasing acyl donor concentration was also observed for microsomal recombinant WT CsDGAT1B and its variants at lower oleoyl-CoA concentrations (Fig. 5D) with the Hill coefficient values ranged from 1.35 to 2.18. Similar to the BnaDGAT1 variants, there were no differences in $S_{0.5}$ values based on kinetic data from microsomal recombinant WT CsDGAT1B and its variants.

A model which takes into consideration both sigmoidal and substrate inhibition kinetics

The observation of both sigmoidal and substrate inhibition kinetics for BnaDGAT1 and CsDGAT1B suggests that these DGAT1s are regulated by their substrates. Indeed, the classical sigmoidal (Equation 1) or substrate inhibition (Equation 2) model alone is not ideal for the prediction of the enzyme kinetics of the observed behaviours of BnaDGAT1 or CsDGAT1B. Thus, a new kinetic model (24) which takes into account both substrate inhibition and sigmoidicity shown in Equation 3.

$$v = \frac{V_{max} \times S^n}{S_{0.5}^n + S^n} \qquad \text{(Equation 1)}$$

where v represents the reaction velocity, S represents the substrate concentration, $S_{0.5}$ represents the substrate concentration resulting at 50% of V_{max}, and n represents the Hill coefficient.

$$v = \frac{V_{max} \times S}{K_m + S \times (1 + \frac{S}{K_i})} \qquad \text{(Equation 2)}$$

where v represents the reaction velocity, S represents the substrate concentration, K_m represents the substrate concentration resulting at 50% of V_{max}, and K_i represents the inhibition constant.

$$v = \frac{V_{max} \times S^n}{K_m^n + S^n \times (1 + \frac{S}{K_i})} \quad \text{(Equation 3)}$$

where v represents the reaction velocity, S represents the substrate concentration, K_m represents the substrate concentration resulting at 50% of V_{max}, K_i represents the inhibition constant, and n represents the Hill coefficient.

This model predicts an initial lag in activity (sigmoidal) before reaching maximum activity, which is followed by a gradual reduction in activity due to the impact of substrate inhibition effect (Fig. 6). This model resulted in a better fit for the kinetics of all DGAT1 variants (similar or slightly higher R^2, Table S1) when compared with the results obtained from substrate inhibition model (Fig. 3 and Fig. 5).

Discussion

Amino acid residue substitutions in DGAT leading to enhanced activity have been reported in DGAT1s from maize (11), *Tropaeolum majus* (25), *Corylus americana* and soybean (10). However, due to the absence of a three-dimensional structure of this enzyme, the exact mechanisms for the effect of the beneficial amino acid residue substitutions on DGAT function remain elusive. It has been suggested that the amino acid residues potential affecting enzyme function may be far away from each other in the amino acid sequence (10) but may in fact move closely to each other to contribute to the active site after polypeptide folding.

Recently, PTMD9 of BnaDGAT1 was shown to contain key amino acid residues influencing the activity of the enzyme (17). Amino acid residue substitutions in recombinant BnaDGAT1-PTMD9 variants generated through directed evolution resulted in increased neutral lipid accumulation in *S. cerevisiae* strain 4 delta. In the current study, the effect of amino acid residue substitutions in PTMD9 on DGAT1 performance was investigated. None of the amino acid residue substitutions of the studied BnaDGAT1 variants resides in the putative functional motifs of DGAT1 (14) and the substitutions were between the amino acid residues with similar properties. Three BnaDGAT1 variants with amino acid residue substitutions in PTMD9 (L441P, I447F or F449C) and one out-group variant V125F were characterized in detail by analyzing their enzyme activities, production levels and enzyme kinetics. As shown in Fig 1, 2 and S2, BnaDGAT1 variants were found to boost neutral lipid production in the yeast transformants for different reasons. The amino acid residue substitutions affected BnaDGAT1 activity and/or polypeptide production. Variant L441P exhibited increased activity whereas variant I447F accumulated to higher levels than WT BnaDGAT1. In contrast, variant F449C exhibited both increased enzyme activity and poly peptide accumulation. These differences occurred despite the fact that amino

acid residues 441, 447 and 449 were in close proximity in PTMD9. It should be noted that the increased enzyme activity for these variants during the log phase was not tightly associated with changes in the level of polypeptide accumulation (Fig. 2). Since the DGAT assay was conducted using yeast 4 delta microsomal fractions, it is possible that the measured enzyme activity was affected by variations in the endogenous DAG content of the microsomes even though a relatively high amount of exogenous DAG was added to the reaction mixture.

The increased BnaDGAT1 polypeptide accumulation observed for variant I447F and F449C (Fig. 1 and 2) may be related to enhanced protein synthesis and/or the increased cellular stability of the variant polypeptide. The expression of WT *BnaDGAT1* and its variants may also be controlled by transcriptional regulation. Even though expression and plasmid copy number of WT *BnaDGAT1* and that of its variants in yeast were at similar levels (Fig. S3), we still cannot completely rule out the possibility of variations in cDNA expression affecting polypeptide accumulation levels, especially considering the *BnaDGAT1* variants were carried by a high copy plasmid and expressed under the control of the strong *Gal1* promoter. For BnaDGAT1 variants with increased activity (e.g., L441P), in addition to contributing to a more favourable conformation in support of catalysis, it is also possible that the increased enzyme activity may be related to an altered interaction with a hypothetical modulator. Indeed, certain protein partners and modulatory molecules have been shown to be required for DGAT function (14, 26–29). It is also known that DGATs can be regulated at post-translational level via phosphorylation and/or ubiquitination (25, 30). Putative phosphorylation and ubiquitination sites in BnaDGAT1 were predicted by NetPhosK (31) and UnPred (32), respectively, and among the selected variants only residue K110 is identified to be related to ubiquitination. No differences in protein accumulation were observed, however, between variant K110N/L441P and L441P (data not shown). It should also be noted that SDS-PAGE and subsequent western blotting of microsomal proteins, prepared from yeast cells harvested at different culture times, did not reveal additional polypeptide fragments lower in molecular mass than full length BnaDGAT1 (or the variants examined) suggesting that the enzyme was subject to little or no proteolysis. Nonetheless, it would be worthwhile to conduct a comprehensive study on the effects of amino acid residue substitutions on the protein stability of the BnaDGAT1 variants.

The enzyme kinetics of BnaDGAT1 were also affected by amino acid residue substitutions in PTMD9. When enzyme activity was determined at increasing acyl-CoA concentration, an eventual decrease in enzyme activity was observed for variant V125F, I447F, F449C, or WT BnaDGAT1 (Fig. 3A, B, D, E). This might be explained by the effect of substrate inhibition. Previously, many acyl-CoA-dependent enzymes (33–38), including DGATs (39–41), have been found to be inhibited at relatively high concentrations of acyl donor. It

is interesting to note that L441P displayed high activity at all oleoyl-CoA concentrations examined (Fig. 3C), suggesting that this enzyme variant may have a better tolerance of increasing oleoyl-CoA. An eventual decrease (to around 45% of the activity at 15 μM oleoyl-CoA) in enzyme activity, however, was observed for L441P with further increase in oleoyl-CoA concentration to 60 μM (data not shown). The formation of acyl-CoA micelles (42) and the inhibition of enzyme activity by detergent effect of acyl-CoA (39) might occur at such high concentration, together with substrate inhibition resulting in the final decrease in enzyme activity. In other examples, the removal of substrate inhibition led to a concomitant decrease in enzyme activity and/or increase in K_m value (43). Compared with WT BnaDGAT1, variant L441P displayed weak substrate inhibition accompanied by increased activity and similar K_m value (Table 1). Variant L441P may be particularly useful for increasing seed oil content when combined with a strategy for increasing the concentration of the acyl-CoA pool.

The beneficial amino acid residue substitutions in BnaDGAT1-PTMD9 are conserved among various species (L441 and I447F, Fig. 4), suggesting that the knowledge generated from BnaDGAT1 variants might be transferred to other DGAT1s. Introducing the equivalent amino acid residue substitutions into CsDGAT1B resulted in enhanced neutral lipid accumulation in yeast 4 delta (Fig. 5A), which may be explained by the increased performance of the CsDGAT1B variants relative to that of WT CsDGAT1B (Fig. 5B). CsDGAT1B and its variants were found to exhibit substrate inhibition kinetics (Fig. 5C) and more importantly, CsDGAT1B variant L460P (Table 2) also displayed the improved catalytic properties (decreased substrate inhibition and increased enzyme activity). Together, the similarity in enzyme activity effects and kinetics between BnaDGAT1 variants and the corresponding CsDGAT1B variants demonstrated that the beneficial amino acid residue substitutions in BnaDGAT1 could be transferred to a DGAT1 from another plant species.

Sigmoidal kinetics for BnaDGAT1, CsDGAT1B and their variants were observed at lower oleoyl-CoA concentrations (Fig. 3F-J and Fig. 5D). The observed sigmoidal kinetics is consistent with a recent investigation of the allosteric properties of WT BnaDGAT1 (44). In addition, Roesler et al. (10) reported the sigmoidal kinetics for DGAT1s from *C. americana* and maize when varying the oleoyl-CoA concentration (0.1-5 μM for *C. americana* DGAT1 and 1-10 μM for maize DGAT1). The investigators modified *C. americana* DGAT1 by DNA shuffling and identified nine kinetically improved *C. americana* DGAT1 variants with increased substrate affinity and/or cooperativity (10). However, unlike Roesler et al. (10), the current study did not identify any trends in $S_{0.5}$ or Hill coefficient values for the BnaDGAT1 (or CsDGAT1B) variants compared with WT BnaDGAT1 (or CsDGAT1B). This discrepancy might be explained by the difference in the degree of modification of the DGAT1 sequence. In our study, error-prone PCR

was used to introduce mutations and by controlling the reaction conditions, the mean number of amino acid residue substitutions was estimated to be less than 3.8 in the resulting BnaDGAT1 variants (4). The BnaDGAT1 and CsDGAT1B variants examined only contained one or two amino acid residue substitutions. These very limited changes in amino acid sequence may not have resulted in large changes in enzyme conformation. In contrast, the *C. americana* DGAT1 variants generated by Roesler et al. (10) contained 6 to 17 amino acid residue substitutions, probably resulting in more extensive effects on enzyme conformation and subsequent impacts on kinetic parameters. In addition, it would be useful to purify the most interesting BnaDGAT1 variants for additional kinetic studies under conditions where the variants are not potentially influenced by other proteins in the microsomes.

The combined substrate activation and inhibition kinetics observed for the WT plant DGAT1s and the variants might be explained by the presence of more than one acyl-CoA binding sites in the enzyme. Sigmoidal kinetics suggest that there is a cooperative effect when more than one substrate molecule binds to an allosteric enzyme (45). In addition to the proposed acyl-CoA binding motif FYXDWWN in the hydrophobic segment (46), the hydrophilic N-terminal domain has been shown to associate with acyl-CoA via an allosteric interaction (14, 20, 21, 44). Substrate inhibition could potentially arise when two substrate molecules bind to the enzyme to form a catalytically inactive ES2 complex by blocking second substrate binding (24) or product release (47), or when the substrate binding leads to the formation of less thermodynamically favoured ES complex that turns over slowly (48–50). In this study, it is hypothesized that the substrate inhibition of plant DGAT1 is caused by the formation of ES2 complex. This assumption is supported by the decrease in substrate inhibition observed when replacing the bulky aliphatic Leu 441 in BnaDGAT1, or Leu 460 in CsDGAT1B with Pro (Fig. 3 and 5), which might disturb the further binding of acyl-CoA to ES complex. It should be noted that the inhibition of DGAT activity observed at higher concentrations of acyl-CoA probably does not involve the allosteric acyl-CoA binding site in the hydrophilic N-terminal domain of BnaDGAT1 since a truncation of BnaDGAT1, devoid of the hydrophilic N-terminal domain, also displayed substrate inhibition (44). Detailed structural information will be necessary to gain more insight into how the amino acid residue substitutions in BnaDGAT1 contribute to changes in the degree of substrate inhibition.

In conclusion, our results suggested that the beneficial amino acid residue substitutions in BnaDGAT1-PTMD9 led to enhanced enzyme performance in yeast via different mechanisms. The increased TAG accumulation in yeast producing these variants was due to variant enzymes with increased enzyme activity, increased protein accumulation and/or reduced substrate inhibition. We also demonstrated that the beneficial amino acid residue substitutions in a DGAT1 from one species improved a DGAT1

from another species, which points out the possibility of systematically engineering of DGAT1 by taking the advantage of the amino acid residue substitution database generated based on the BnaDGAT1 variants. The fact that a single amino acid residue substitution can lead to an improved DGAT1 suggests that non-transgenic approaches such as Targeting-Induced Local Lesions IN Genomes (TILLING) (51) or clustered regularly interspaced short palindromic repeats (CRISPR) (52) may represent useful methods for improving DGAT action *in planta*. Indeed, genome editing has recently been used to introduce loss-of-function mutations into *DGAT1* and *PHOSPHOPLIPID:DIACYLGLYCEROL ACYLTRANSFERASE* genes in *C. sativa*, thereby leading to a reduction in seed TAG content (53).

Experimental procedures

Construct preparation, yeast transformation and heterologous expression of DGAT1 variants

BnaDGAT1 variants together with WT *BnaDGAT1* were re-cloned into the pYES2.1/V5-His TOPO yeast expression vector (Invitrogen, Burlington, ON, Canada), under the control of the galactose-inducible *GAL1* promoter. The stop codon of each gene was eliminated from the sequences for in-frame fusion with a C-terminal V5 tag encoded on the pYES2.1/V5-His TOPO vector. The *CsDGAT1* variants were chemically synthesized by Invitrogen and inserted into the pYES2.1 vector.

After the integrity of all constructs was confirmed by sequencing, they were transformed into the quadruple mutant strain *S. cerevisiae* H1246 (4 delta, *MATα are1-Δ::HIS3, are2-Δ::LEU2, dga1-Δ::KanMX4, lro1-Δ::TRP1 ADE2*) using an *S.c.* EasyComp Transformation Kit (Invitrogen). Yeast transformed with *pYES-LacZ* was used as a control. The recombinant yeast cells were first grown in liquid minimal medium (0.67% (w/v) yeast nitrogen base and 0.2 % (w/v) SC-Ura) with 2% (w/v) raffinose for 24 h. An aliquot of the yeast cell culture (at a starting OD_{600} value of 0.4) was used to inoculate minimal medium containing 2% (w/v) galactose and 1% (w/v) raffinose (referred as induction medium). Cultures for all experiments were grown at 30°C with shaking at 220 rpm. In order to generate time-course production profiles for the various BnaDGAT1 variants, cells were harvested by centrifugation (at 3000 g for 5 min at 4°C) every 2 h starting at the OD_{600} of 5 until the stationary growth phase.

Analysis of neutral lipid content in yeast

The Nile Red fluorescence assay was conducted as described previously (18). Yeast cultures were aliquoted (100 μL per well) into 96-well solid black plates (Corning Inc., Corning, NY, USA) and incubated with 5 μL of Nile Red solution (0.1 mg/mL in methanol) for 30 s at room temperature. The fluorescence was measured before and after the addition of Nile Red solution with excitation at 485 nm and emission at 538 nm using a Synergy H4 Hybrid reader (Biotek, Winooskit, VT, USA). The Nile Red values were calculated based on the change in fluorescence over OD_{600} ($\Delta F/OD_{600}$).

Microsome extraction

Microsomal fractions were isolated from recombinant yeast cells as described previously (18). In brief, the recombinant yeast cells were resuspended in 1 mL of lysis buffer (20 mM Tris-HCl pH 7.9, containing 10 mM $MgCl_2$, 1 mM EDTA, 5% (v/v) glycerol, 300 mM ammonium sulfate and 2 mM dithiothreitol), and homogenized in the presence of 0.5 mm glass beads by a bead beater (Biospec, Bartlesville, OK, USA). The crude homogenate was centrifuged at 10 000 g for 30 min to sediment cell debris and glass beads. The supernatant was transferred into an ultracentrifuge tube and centrifuged at 105 000 g for 70 min to pellet the microsomes using an ultracentrifuge (Optima MAX-XP, Beckman-Coulter, Mississauga, ON, Canada). The resulting microsomal fraction was resuspended in 3 mM imidazole buffer (pH 7.4) containing 125 mM sucrose. All procedures were conducted at 4°C. The concentration of crude protein was quantified by the Bradford assay (Bio-Rad, Mississauga, ON, Canada) using BSA as a standard (54).

In vitro DGAT1 activity assay

The DGAT assay was conducted according to the procedure described previously (13). Briefly, the assay mixture (60 μL) contained 200 mM HEPES-NaOH (pH 7.4), 3.2 mM $MgCl_2$, 333 μM *sn*-1,2-diolein dispersed in 0.2% (v/v) Tween 20, 15 μM [1-^{14}C] oleoyl-CoA (55 μCi/μmol; PerkinElmer, Waltham, MA, USA), and 2 μg of microsomal protein. The reaction was initiated by adding microsomes containing recombinant DGAT1 variants and incubated at 30°C for 4 min with shaking before quenching with 10 μL of 10% (w/v) SDS. The entire reaction mixture was spotted onto a thin-layer chromatography (TLC) plate (0.25 mm Silica gel, DC-Fertigplatten, Macherey-Nagel, Germany) and the plate was developed with hexane/diethyl ether/acetic acid (80:20:1, v/v/v). The resolved lipids were visualized by phosphorimaging (Typhoon Trio Variable Mode Imager, GE Healthcare, Mississauga, ON, Canada) and corresponding TAG spots were scraped, and radioactivity was quantified by a LS 6500 multi-purpose scintillation counter (Beckman-Coulter).

For kinetic studies of recombinant BnaDGAT1 variants, enzyme assays were allowed to proceed for 1 min using 0.2 μg of microsomal protein. Recombinant CsDGAT1B variants were assayed for 4 min and the quantity of microsomal protein used was as follows: for WT CsDGAT1B, 10 μg of microsomal protein; I144F and I466F, 2.5 μg of microsomal protein; L460P and L460P/I466F, 1 μg of microsomal protein. The concentration of [1-^{14}C] oleoyl-CoA was varied from 0.1 to 25 μM while *sn*-1,2-diolein were held constant at 333 μM. Kinetic parameters were calculated by fitting the data to the Michaelis-Menten, substrate inhibition or allosteric sigmoidal equations using the program GraphPad Prism (version 6.0; GraphPad Software, La Jolla, CA, USA).

Western blotting

Equivalent amounts of microsomal proteins (10 μg) from yeast strain 4 delta producing recombinant

BnaDGAT1 variants and LacZ were resolved using 8-16% gradient Mini-Protean TGX Precast Gels (Bio-Rad) and electrotransferred (overnight at 30 mA and 4°C) onto polyvinylidene difluoride membrane (Amersham, GE Healthcare). The target C-terminal-tagged recombinant BnaDGAT1 variants were detected using anti-V5-HRP conjugated antibody (Invitrogen). To ensure equal protein loading, yeast constitutively producing Kar2p protein was used as an internal standard. Kar2p polypeptide was detected using a rabbit polyclonal anti-Kar2p (Santa Cruz Biotechnology, Santa Cruz, CA, USA) as the primary antibody followed by HRP goat anti-rabbit IgG (H+L) secondary antibody (Invitrogen). Both HRP conjugated antibodies were detected by chemiluminescence (FluorChem SP, Alpha Innotech Corp., San Leandro, CA, USA) using an ECL Advance Western Blotting Detection Kit (Amersham). The band densities of BnaDGAT1 variants and internal standard were quantified with ImageJ software (55). The relative DGAT polypeptide accumulation level was calculated based on the density of the DGAT band after normalizing to internal standard.

Quantitative RT-PCR

Quantitative RT-PCR (qPCR) was performed on a StepOnePlus Real-Time PCR System (Applied Biosystems, Foster, CA, USA) using the Platinum SYBR Green qPCR Master Mix (Invitrogen) as described previously (56).

Plasmid copy number assay-Plasmid copy numbers were quantified according to Karim et al. (57). Total DNA was extracted using glass bead beating followed by phenol-chloroform extraction (58). Plasmid copy number was calculated using the standard curve method. To quantify the copy number, a section of the *BnaDGAT1* gene (avoiding the mutated region) on the plasmid was targeted (with primers 5'-GGCCAATCCTGAAGTCTCCTACT-3' and 5'-TGGGAGCAAGCATGAAATACG-3') and compared to a genomic target in the single copy *ScALG9* gene (Saccharomyces Genome Database (SGD) ID: S000005163, with primers 5'-GCCGTTGCCATGTTGTTGTA-3' and 5'-GACCCAGTGGACAGATAGCG-3'). Standard curves were created using plasmid containing both *BnaDGAT1* and *ScALG9* genes in the pYES2.1 vector. A serial dilution of this plasmid with concentration ranging from 5×10^2 to 5×10^7 copies per μL was used to create standard curves for both *BnaDGAT1* and *ScALG9*. Copy number here refers to the copy number per haploid genome rather than per cell considering there are two copies of genome per cell during certain phases of cell division.

Gene expression analysis-Gene expression of *BnaDGAT1* and its variants in yeast was analyzed as follows. Total RNA was isolated from yeast cells at the mid-log phase using the RNeasy kit according to the manufacturer's instruction (Qiagen, Toronto, ON, Canada). First-strand cDNA was synthesized in a 10-μL reaction mixture with 1 μg of total RNA using the SuperScript III first-strand cDNA synthesis kit (Invitrogen). The relative expression levels of the

BnaDGAT1 variants in yeast were calculated using the comparative Ct method ($2^{-\Delta\Delta Ct}$ method) (59). The results are presented as fold differences in gene expression after normalizing to the yeast stably expressing *ScACT1* gene (SGD ID: S000001855). cDNA of variant V333I was used as a calibrator to normalize for plate-to-plate variation. The primers for *BnaDGAT1* and its variants were the same as the primers we used to quantify plasmid copy number. The primers for *ScACT1* cDNA were 5'-TCGTTCCAATTTACGCTGGTT-3' and 5'-CGGCCAAATCGATTCTCAA-3'.

Amino acid sequence analysis

Multiple amino acid sequence alignments of 43 DGAT1 proteins from different species (Table S2) were conducted using ClustalW in MEGA 7 with default settings (60). The alignment was used to construct a neighbour-joining tree using the same software with 1000 bootstrap repetitions. The topology organization of BnaDGAT1 was predicted using Phobius (61).

Statistical analysis

All experiments were repeated at least twice (n = the number of independent experiments). Data are shown as means ± standard deviation (S.D.) when $n \geq 3$, or mean ± range when n = 2, unless otherwise stated. Statistical analysis was performed using a one-way analysis of variance (ANOVA), and mean separation was determined using the LSD test using the SPSS statistical package (SPSS 16.0, Chicago, IL, USA). Means were considered significantly different at $P < 0.05$.

Acknowledgments

We thank Dr. Sten Stymne from Swedish University of Agricultural Sciences for providing yeast strain H1246.

Conflict of interest

The authors declare that they have no conflicts of interest with the content of this article.

Author contributions

YX performed all experiments, analyzed the data and prepared the initial draft of the manuscript. RJW, YX and GC designed the research approach. GR isolated the cDNA of *CsDGAT1B* and designed *CsDGAT1B* variants. GC, MSG and KMPC contributed valuable discussion during this study. All co-authors contributed to further editing of the manuscript.

References

1. Dyer, J. M., Stymne, S., Green, A. G., and Carlsson, A. S. (2008) High-value oils from plants. *Plant J.* **54**, 640–655
2. Biermann, U., Bornscheuer, U., Meier, M. A. R., Metzger, J. O., and Schäfer, H. J. (2011) Oils and fats as renewable raw materials in chemistry. *Angew. Chemie Int. Ed.* **50**, 3854–3871
3. Chapman, K. D., and Ohlrogge, J. B. (2012) Compartmentation of triacylglycerol accumulation in plants. *J. Biol. Chem.* **287**, 2288–2294
4. Siloto, R. M. P., Truksa, M., Brownfield, D., Good, A. G., and Weselake, R. J. (2009) Directed evolution of acyl-CoA:diacylglycerol acyltransferase: development and characterization of *Brassica napus* DGAT1 mutagenized libraries. *Plant Physiol. Biochem.* **47**, 456–461
5. Lung, S. C., and Weselake, R. J. (2006) Diacylglycerol acyltransferase: a key mediator of plant triacylglycerol synthesis. *Lipids*. **41**, 1073–1088
6. Harwood, J. L., Ramli, U. S., Tang, M., Quant, P. A., Weselake, R. J., Fawcett, T., and Guschina, I. A. (2013) Regulation and enhancement of lipid accumulation in oil crops: The use of metabolic control analysis for informed genetic manipulation. *Eur. J. Lipid Sci. Technol.* **115**, 1239–1246
7. Weselake, R. J., Shah, S., Tang, M., Quant, P. A., Snyder, C. L., Furukawa-Stoffer, T. L., Zhu, W., Taylor, D. C., Zou, J., Kumar, A., Hall, L., Laroche, A., Rakow, G., Raney, P., Moloney, M. M., and Harwood, J. L. (2008) Metabolic control analysis is helpful for informed genetic manipulation of oilseed rape (*Brassica napus*) to increase seed oil content. *J. Exp. Bot.* **59**, 3543–3549
8. Taylor, D. C., Zhang, Y., Kumar, A., Francis, T., Giblin, E. M., Barton, D. L., Ferrie, J. R., Laroche, A., Shah, S., Zhu, W., Snyder, C. L., Hall, L., Rakow, G., Harwood, J. L., and Weselake, R. J. (2009) Molecular modification of triacylglycerol accumulation by over-expression of DGAT1 to produce canola with increased seed oil content under field conditions. *Botany*. **87**, 533–543
9. Lardizabal, K., Effertz, R., Levering, C., Mai, J., Pedroso, M. C., Jury, T., Aasen, E., Gruys, K., and Bennett, K. (2008) Expression of *Umbelopsis ramanniana* DGAT2A in seed increases oil in soybean. *Plant Physiol.* **148**, 89–96
10. Roesler, K., Shen, B., Bermudez, E., Li, C., Hunt, J., Damude, H. G., Ripp, K. G., Everard, J. D., Booth, J. R., Castaneda, L., Feng, L., and Meyer, K. (2016) An improved variant of soybean type 1 diacylglycerol acyltransferase increases the oil content and decreases the

soluble carbohydrate content of soybeans. *Plant Physiol.* **171**, 878–893

11. Zheng, P., Allen, W. B., Roesler, K., Williams, M. E., Zhang, S., Li, J., Glassman, K., Ranch, J., Nubel, D., Solawetz, W., Bhattramakki, D., Llaca, V., Deschamps, S., Zhong, G. Y., Tarczynski, M. C., and Shen, B. (2008) A phenylalanine in DGAT is a key determinant of oil content and composition in maize. *Nat. Genet.* **40**, 367–372
12. Misra, A., Khan, K., Niranjan, A., Nath, P., and Sane, V. A. (2013) Over-expression of JcDGAT1 from *Jatropha curcas* increases seed oil levels and alters oil quality in transgenic *Arabidopsis thaliana*. *Phytochemistry*. **96**, 37–45
13. Caldo, K. M. P., Greer, M. S., Chen, G., Lemieux, M. J., and Weselake, R. J. (2015) Purification and properties of recombinant *Brassica napus* diacylglycerol acyltransferase 1. *FEBS Lett.* **589**, 773–778
14. Liu, Q., Siloto, R. M. P., Lehner, R., Stone, S. J., and Weselake, R. J. (2012) Acyl-CoA:diacylglycerol acyltransferase: molecular biology, biochemistry and biotechnology. *Prog. Lipid Res.* **51**, 350–377
15. Cheng, F., Zhu, L., and Schwaneberg, U. (2015) Directed evolution 2.0: improving and deciphering enzyme properties. *Chem. Commun.* **51**, 9760–9772
16. Packer, M. S., and Liu, D. R. (2015) Methods for the directed evolution of proteins. *Nat. Rev. Genet.* **16**, 379–394
17. Chen, G., Xu, Y., Siloto, R. M. P., Caldo, K. M. P., Vanhercke, T., Tahchy, A. El, Niesner, N., Chen, Y., Mietkiewska, E., and Weselake, R. J. (2017) High performance variants of plant diacylglycerol acyltransferase 1 generated by directed evolution provide insights into structure-function. *Plant J.* doi: 10.1111/tpj.13652
18. Siloto, R. M. P., Truksa, M., He, X., McKeon, T., and Weselake, R. J. (2009) Simple methods to detect triacylglycerol biosynthesis in a yeast-based recombinant system. *Lipids*. **44**, 963–973
19. Faergeman, N. J., and Knudsen, J. (1997) Role of long-chain fatty acyl-CoA esters in the regulation of metabolism and in cell signalling. *Biochem. J.* **323**, 1–12
20. Siloto, R. M. P., Madhavji, M., Wiehler, W. B., Burton, T. L., Boora, P. S., Laroche, A., and Weselake, R. J. (2008) An N-terminal fragment of mouse DGAT1 binds different acyl-CoAs with varying affinity. *Biochem. Biophys. Res. Commun.* **373**, 350–354
21. Weselake, R. J., Madhavji, M., Szarka, S. J., Patterson, N. A., Wiehler, W. B., Nykiforuk, C. L., Burton, T. L., Boora, P. S., Mosimann, S. C., Foroud, N. A., Thibault, B. J., Moloney, M. M., Laroche, A., and Furukawa-Stoffer, T. L. (2006) Acyl-CoA-binding and self-associating properties of a recombinant 13.3 kDa N-terminal fragment of diacylglycerol acyltransferase-

1 from oilseed rape. *BMC Biochem.* **7**, 24

22. Bansal, S., and Durrett, T. P. (2015) *Camelina sativa*: An ideal platform for the metabolic engineering and field production of industrial lipids. *Biochimie*. **120**, 9–16
23. Kim, H., Hyun, J., Da, P., Kim, J., and Yonghwi, A. (2016) Functional analysis of *diacylglycerol acyltransferase1* genes from *Camelina sativa* and effects of *CsDGAT1B* overexpression on seed mass and storage oil content in *C. sativa*. *Plant Biotechnol. Rep.* **10**, 141–153
24. Dovala, D., Rath, C. M., Hu, Q., Sawyer, W. S., Shia, S., Elling, R. A., Knapp, M. S., and Metzger, L. E. (2016) Structure-guided enzymology of the lipid A acyltransferase LpxM reveals a dual activity mechanism. *Proc. Natl. Acad. Sci. U. S. A.* **113**, E6064–E6071
25. Xu, J., Francis, T., Mietkiewska, E., Giblin, E. M., Barton, D. L., Zhang, Y., Zhang, M., and Taylor, D. C. (2008) Cloning and characterization of an acyl-CoA-dependent diacylglycerol acyltransferase 1 (DGAT1) gene from *Tropaeolum majus*, and a study of the functional motifs of the DGAT protein using site-directed mutagenesis to modify enzyme activity and oil content. *Plant Biotechnol. J.* **6**, 799–818
26. Jin, Y., McFie, P. J., Banman, S. L., Brandt, C. J., and Stone, S. J. (2014) Diacylglycerol acyltransferase-2 (DGAT2) and monoacylglycerol acyltransferase-2 (MGAT2) interact to promote triacylglycerol synthesis. *J. Biol. Chem.* **289**, 28237–28248
27. Gidda, S. K., Shockey, J. M., Falcone, M., Kim, P. K., Rothstein, S. J., Andrews, D. W., Dyer, J. M., and Mullen, R. T. (2011) Hydrophobic-domain-dependent protein-protein interactions mediate the localization of GPAT enzymes to ER subdomains. *Traffic*. **12**, 452–472
28. Xu, N., Zhang, S. O., Cole, R. A., McKinney, S. A., Guo, F., Haas, J. T., Bobba, S., Farese, R. V, and Mak, H. Y. (2012) The FATP1-DGAT2 complex facilitates lipid droplet expansion at the ER-lipid droplet interface. *J. Cell Biol.* **198**, 895–911
29. Man, W. C., Miyazaki, M., Chu, K., and Ntambi, J. (2006) Colocalization of SCD1 and DGAT2: implying preference for endogenous monounsaturated fatty acids in triglyceride synthesis. *J. Lipid Res.* **47**, 1928–1939
30. Brandt, C., McFie, P. J., and Stone, S. J. (2016) Biochemical characterization of human acyl coenzyme A: 2-monoacylglycerol acyltransferase-3 (MGAT3). *Biochem. Biophys. Res. Commun.* **475**, 264–270
31. Blom, N., Sicheritz-Pontén, T., Gupta, R., Gammeltoft, S., and Brunak, S. (2004) Prediction of post-translational glycosylation and phosphorylation of proteins from the amino acid sequence. *Proteomics*. **4**, 1633–1649

32. Radivojac, P., Vacic, V., Haynes, C., Cocklin, R. R., Mohan, A., Heyen, J. W., Goebl, M. G., and Iakoucheva, L. M. (2010) Identification, analysis, and prediction of protein ubiquitination sites. *Proteins Struct. Funct. Bioinforma.* **78**, 365–380

33. Cao, J., Lockwood, J., Burn, P., and Shi, Y. (2003) Cloning and functional characterization of a mouse intestinal acyl-CoA:monoacylglycerol acyltransferase, MGAT2. *J. Biol. Chem.* **278**, 13860–13866

34. Soupene, E., Fyrst, H., and Kuypers, F. A. (2008) Mammalian acyl-CoA:lysophosphatidylcholine acyltransferase enzymes. *Proc. Natl. Acad. Sci. U. S. A.* **105**, 88–93

35. Soupene, E., Wang, D., and Kuypers, F. A. (2015) Remodeling of host phosphatidylcholine by *Chlamydia* acyltransferase is regulated by acyl-CoA binding protein ACBD6 associated with lipid droplets. *Microbiologyopen*. **4**, 235–251

36. Bafor, M., Stobart, A. K., and Stymne, S. (1990) Properties of the glycerol acylating enzymes in microsomal preparations from the developing seeds of safflower (*Carthamus tinctorius*) and turnip rape (*Brassica campestris*) and their ability to assemble cocoa-butter type fats. *J. Am. Oil Chem. Soc.* **67**, 217–225

37. Ruiz-López, N., Garcés, R., Harwood, J. L., and Martínez-Force, E. (2010) Characterization and partial purification of acyl-CoA:glycerol 3-phosphate acyltransferase from sunflower (*Helianthus annuus L.*) developing seeds. *Plant Physiol. Biochem.* **48**, 73–80

38. Salas, J. J., Martínez-Force, E., Harwood, J. L., Venegas-Calerón, M., Aznar-Moreno, J. A., Moreno-Pérez, A. J., Ruíz-López, N., Serrano-Vega, M. J., Graham, I. A., Mullen, R. T., and Garcés, R. (2014) Biochemistry of high stearic sunflower, a new source of saturated fats. *Prog. Lipid Res.* **55**, 30–42

39. Stöveken, T., Kalscheuer, R., Malkus, U., Reichelt, R., and Steinbüchel, A. (2005) The wax ester synthase/acyl coenzyme A:diacylglycerol acyltransferase from *Acinetobacter* sp. strain ADP1: characterization of a novel type of acyltransferase. *J. Bacteriol.* **187**, 1369–1376

40. Chung, M. Y., Rho, M. C., Lee, S. W., Park, H. R., Kim, K., Lee, I. A., Kim, D. H., Jeune, K. H., Lee, H. S., and Kim, Y. K. (2006) Inhibition of diacylglycerol acyltransferase by betulinic acid from *Alnus hirsuta*. *Planta Med.* **72**, 267–269

41. Ganji, S. H., Tavintharan, S., Zhu, D., Xing, Y., Kamanna, V. S., and Kashyap, M. L. (2004) Niacin noncompetitively inhibits DGAT2 but not DGAT1 activity in HepG2 cells. *J. Lipid Res.* **45**, 1835–1845

42. Little, D., Weselake, R., Pomeroy, K., Furukawa-Stoffer, T., and Bagu, J. (1994) Solubilization and characterization of diacylglycerol acyltransferase from microspore-

derived cultures of oilseed rape. *Biochem. J.* **304**, 951–958

43. Ziegler, J., Brandt, W., Geißler, R., and Facchini, P. J. (2009) Removal of substrate inhibition and increase in maximal velocity in the short chain dehydrogenase/reductase salutaridine reductase involved in morphine biosynthesis. *J. Biol. Chem.* **284**, 26758–26767
44. Caldo, K.M.P., Acedo, J.Z., Panigrahi, R., Vederas, J.C., Weselake, R.J. and Lemieux, M.J. (2017) Diacylglycerol acyltransferase 1 is regulated by its N-terminal domain in response to allosteric effectors. *Plant Physiol*, pp-00934.
45. Cohen, G. N. (2014) Allosteric enzymes. In *Microbial biochemistry*, pp. 59–71, Springer Netherlands
46. Lopes, J. L. S., Nobre, T. M., Cilli, E. M., Beltramini, L. M., Araújo, A. P. U., and Wallace, B. A. (2014) Deconstructing the DGAT1 enzyme: Binding sites and substrate interactions. *Biochim. Biophys. Acta*. **1838**, 3145–3152
47. Szegletes, T., Mallender, W. D., Thomas, P. J., and Rosenberry, T. L. (1999) Substrate binding to the peripheral site of acetylcholinesterase initiates enzymatic catalysis. Substrate inhibition arises as a secondary effect. *Biochemistry*. **38**, 122–133
48. Liao, J., Okuyama, M., Ishihara, K., Yamori, Y., Iki, S., Tagami, T., Mori, H., Chiba, S., and Kimura, A. (2016) Kinetic properties and substrate inhibition of α-galactosidase from *Aspergillus niger*. *Biosci. Biotechnol. Biochem.* **80**, 1747–1752
49. Efimov, I., Basran, J., Sun, X., Chauhan, N., Chapman, S. K., Mowat, C. G., and Raven, E. L. (2012) The mechanism of substrate inhibition in human indoleamine 2,3-dioxygenase. *J. Am. Chem. Soc.* **134**, 3034–3041
50. Elamin, A. A., Stehr, M., Spallek, R., Rohde, M., and Singh, M. (2011) The *Mycobacterium tuberculosis* Ag85A is a novel diacylglycerol acyltransferase involved in lipid body formation. *Mol. Microbiol.* **81**, 1577–1592
51. Till, B. J., Zerr, T., Comai, L., and Henikoff, S. (2006) A protocol for TILLING and Ecotilling in plants and animals. *Nat. Protoc.* **1**, 2465–2477
52. Belhaj, K., Chaparro-Garcia, A., Kamoun, S., and Nekrasov, V. (2013) Plant genome editing made easy: targeted mutagenesis in model and crop plants using the CRISPR/Cas system. *Plant Methods*. **9**, 39
53. Aznar-Moreno, J. A., and Durrett, T. P. (2017) Simultaneous targeting of multiple gene homeologs to alter seed oil production in *Camelina sativa*. *Plant Cell Physiol.* 10.1093/pcp/pcx058
54. Bradford, M. M. (1976) A rapid and sensitive method for the quantitation of microgram quantities of protein utilizing the principle of protein-dye binding. *Anal. Biochem.* **72**, 248–

254

55. Schneider, C. A., Rasband, W. S., and Eliceiri, K. W. (2012) NIH Image to ImageJ: 25 years of image analysis. *Nat. Methods*. **9**, 671–675

56. Chen, X., Truksa, M., Snyder, C. L., El-Mezawy, A., Shah, S., and Weselake, R. J. (2011) Three homologous genes encoding sn-glycerol-3-phosphate acyltransferase 4 exhibit different expression patterns and functional divergence in Brassica napus. *Plant Physiol.* **155**, 851–865

57. Karim, A. S., Curran, K. A., and Alper, H. S. (2013) Characterization of plasmid burden and copy number in *Saccharomyces cerevisiae* for optimization of metabolic engineering applications. *FEMS Yeast Res.* **13**, 107–116

58. Lõoke, M., Kristjuhan, K., and Kristjuhan, A. (2011) Extraction of genomic DNA from yeasts for PCR-based applications. *Biotechniques*. **50**, 325–328

59. Livak, K. J., and Schmittgen, T. D. (2001) Analysis of relative gene expression data using real-time quantitative PCR and the 2(−ΔΔC(T)) method. *Methods*. **25**, 402–408

60. Kumar, S., Stecher, G., and Tamura, K. (2016) MEGA7: Molecular Evolutionary Genetics Analysis version 7.0 for bigger datasets. *Mol. Biol. Evol.* **33**, msw054

61. Käll, L., Krogh, A., and Sonnhammer, E. L. L. (2007) Advantages of combined transmembrane topology and signal peptide prediction-the Phobius web server. *Nucleic Acids Res.* **35**, 429–432

Footnotes

The research was supported by Alberta Innovates Bio Solutions, the Natural Science and Engineering Research Council of Canada (RJW, RGPIN-2014-04585; GC, RGPIN-2016-05926) and the Canada Research Chairs Program. We also acknowledge the support of the National Research Strategy BioEconomy Program of the Federal Ministry of Education and Research (Germany), MITACS Elevate Award to GR, and Alberta Innovates Technology Futures. YX is a recipient of a scholarship from the China Scholarship Council and the Alberta Innovates Graduate Student Top-up Award.

The abbreviations used are: DGAT, diacylglycerol acyltransferase; TAG, triacylglycerol; PTMD, predicted transmembrane domain; WT, wild type.

Table 1. Apparent kinetic parameters of BnaDGAT1 variants. Analysis was performed with GraphPad Prism software using the non-linear regression of the substrate inhibition model. Data shown are mean ± S.D, n = 3.

BnaDGAT1 variant	V_{max}^{app} (nmol/min/mg)	K_m^{app} (μM)	K_i^{app} (μM)	DGAT protein abundance in microsomes (relative to BnaDGAT1)	$V_{max'}^{app}$ adjusted for protein abundance (nmol/min/mg)	$V_{max'}^{app}$ / K_m^{app} (mL/min/mg)	$V_{max'}^{app}$ / K_m^{app} relative
BnaDGAT1	6.16 ± 0.32	1.30 ± 0.13	13.42 ± 1.61	1.00	6.16	4.74	1.00
V125F	16.67 ± 1.17	1.73 ± 0.22	11.15 ± 1.60	1.14	14.68	8.49	1.84
L441P	9.94 ± 0.32	1.31 ± 0.10	89.37 ± 18.85	1.02	9.78	7.47	1.62
I447F	8.49 ± 0.52	1.78 ± 0.20	15.00 ± 2.09	1.12	7.55	4.24	0.92
F449C	13.14 ± 0.71	2.23 ± 0.21	18.25 ± 2.33	1.15	11.39	5.11	1.11

Table 2 Apparent kinetic parameters of CsDGAT1B variants. Analysis was performed with GraphPad Prism software using the non-linear regression of the substrate inhibition model. Data are means ± S.D, n = 2 to 3.

CsDGAT1B variant	V_{max}^{app} (nmol/min/mg)	K_m^{app} (μM)	K_i^{app} (μM)
CsDGAT1B	0.09 ± 0.01	0.76 ± 0.14	7.22 ± 1.45
I144F	0.74 ± 0.13	2.24 ± 0.53	2.88 ± 0.71
L460P	0.50 ± 0.03	0.71 ± 0.11	48.64 ± 13.39
I466F	0.32 ± 0.03	0.99 ± 0.15	7.51 ± 1.21
L460P/I466F	0.34 ± 0.03	0.50 ± 0.10	11.61 ± 2.60

Figure legends

Figure 1. Characterization of BnaDGAT1 variants. A. Neutral lipid accumulation in yeasts transformed with different BnaDGAT1 variants. Data are means ± range, n = 2 biological replicates. B. *In vitro* DGAT activities of different BnaDGAT1 variants. Microsomes from yeasts producing recombinant BnaDGAT1 variants were collected at different time points after induction and used for the DGAT assay. The highest microsomal activity of recombinant wild type (WT) BnaDGAT1 was set as 1.0. Growth curve was constructed by measuring OD_{600}. Data are means ± range, n = 2. C, Relative activities of BnaDGAT1 variants. The highest activity of each variant is shown, with recombinant WT BnaDGAT1 activity set as 1.0. Data are means ± range, n = 2. D, Relative protein accumulation level of each variant. Ten μg of microsomal protein from the same batch of microsomes used to assess enzyme activity was used for Western blotting analysis. The relative polypeptide accumulation of recombinant WT BnaDGAT1 was set as 1.0. Data are means ± S.D, n = 3 to 4. E, The normalized relative activity of each enzyme variant was obtained by dividing the enzyme activity value by relative protein accumulation, with recombinant WT BnaDGAT1 activity set as 1.0. Data are means ± S.D, n = 2. The asterisks indicate significant differences in yeast neutral lipid accumulation (A), activity (C), protein accumulation (D), and normalized activity (E) of the yeast/microsomes containing recombinant BnaDGAT1 variants versus those of recombinant WT enzyme (ANOVA, LSD test) at $P < 0.05$ level.

Figure 2. Impact of amino acid residue substitutions in the 9th predicted transmembrane domain of BnaDGAT1 on enzyme activity and accumulation in yeast. A, Production profile of (wild type) WT BnaDGAT1, variants L441P, I447F and F449C. Protein accumulation was determined by Western blotting analysis of microsomal protein of the same batch of cells harvested at different time points. The relative polypeptide accumulation of recombinant WT BnaDGAT1 from the microsomes with highest enzyme activity was set as 1.0. Growth curve was constructed by measuring OD_{600}. Data are means ± range, n = 2. B, Average protein accumulation of each variant. Data are means ± S.D. (n = 4 to 5) of variant protein accumulation in yeast microsomes at different time points. C, Normalized relative activity was calculated by dividing the activity value by the corresponding relative polypeptide accumulation, with the WT BnaDGAT1 normalized activity set as 1.0. Data are means ± S.D. (n = 4 to 5) of normalized activities for yeast microsomes at different time points. For B and C, the results for microsomes harvested at the last time point were not included. The asterisks indicate significant differences protein accumulation (B), and normalized activity (C) of the

microsomes containing recombinant BnaDGAT1 variants versus recombinant WT BnaDGAT1 (ANOVA, LSD test) at $P < 0.05$ level.

Figure 3. Microsomal DGAT activities of BnaDGAT1 variants at increasing oleoyl-CoA concentrations. A-E, DGAT activities of variants at oleoyl-CoA concentration from 0.1 to 25 μM. Data were fitted to a nonlinear regression using substrate inhibition (solid line) and Michaelis-Menten equation (dashed line). F-J, A closer look at BnaDGAT1 kinetics at lower oleoyl-CoA concentration from 0.1 to 5 μM for WT BnaDGAT1, V125F and I447F or from 0.1 to 7.5 μM for L441P and F449C. Data were fitted to a nonlinear regression using allosteric sigmoidal equation (solid line, $R^2>0.96$). Plots were generated with GraphPad Prism. Data points are means ± S.D, n = 3.

Figure 4. Amino acid sequence analysis of DGAT1 proteins from different species. Phylogenetic relationship among protein sequences of DGAT1 were constructed using the neighbour-joining method. Bootstrap values are shown at the tree nodes. The transmembrane domains (TMDs) of BnaDGAT1 were depicted based on the prediction by Phobius. Amino acid alignments of the 9th predicted TMD of each DGAT1 sequence are also indicated. The amino acid residue substitution sites of BnaDGAT1 variants are marked with red-filled triangle.

Figure 5. Characterization of CsDGAT1B variants. A. Neutral lipid accumulation in yeasts 4 delta producing different recombinant CsDGAT1B variants. Data are means ± range, n = 2 to 3 biological replicates. B, Microsomal DGAT activities of recombinant CsDGAT1B variants, with the recombinant (wild type) WT CsDGAT1B activity set as 1.0. Data are means ± range, n = 2. C, DGAT activities of variants at oleoyl-CoA concentrations ranging from 0.1 to 25 μM. Data are means ± S.D, n = 2 to 3. D, CsDGAT1B kinetics at oleoyl-CoA concentration from 0.1 to 1.85 μM. Data are means ± S.D, n = 2 to 3. Plots were generated with GraphPad Prism, and data were fitted to a nonlinear regression using substrate inhibition (B, R^2 between 0.91 and 0.97) or allosteric sigmoidal equation (C, R^2 between 0.96 and 0.99). The asterisks indicate significant differences in neutral lipid accumulation (A) of yeast producing recombinant CsDGAT1B variants or activity of the microsomes containing recombinant CsDGAT1B variants (B) versus the results from the recombinant WT CsDGAT1B (ANOVA, LSD test) at $P < 0.05$ level.

Figure 6. The kinetics of BnaDGAT1 and CsDGAT1B with increasing oleoyl-CoA concentration exhibit a better fit in a kinetic model which accounts for sigmoidicity and substrate inhibition. Plots were generated with GraphPad Prism, and data were fitted to a nonlinear regression using allosteric sigmoidal equation (Equation 1, dashed-dotted line), substrate inhibition (Equation 2, dashed line) or the proposed kinetic model (Equation 3, solid line).

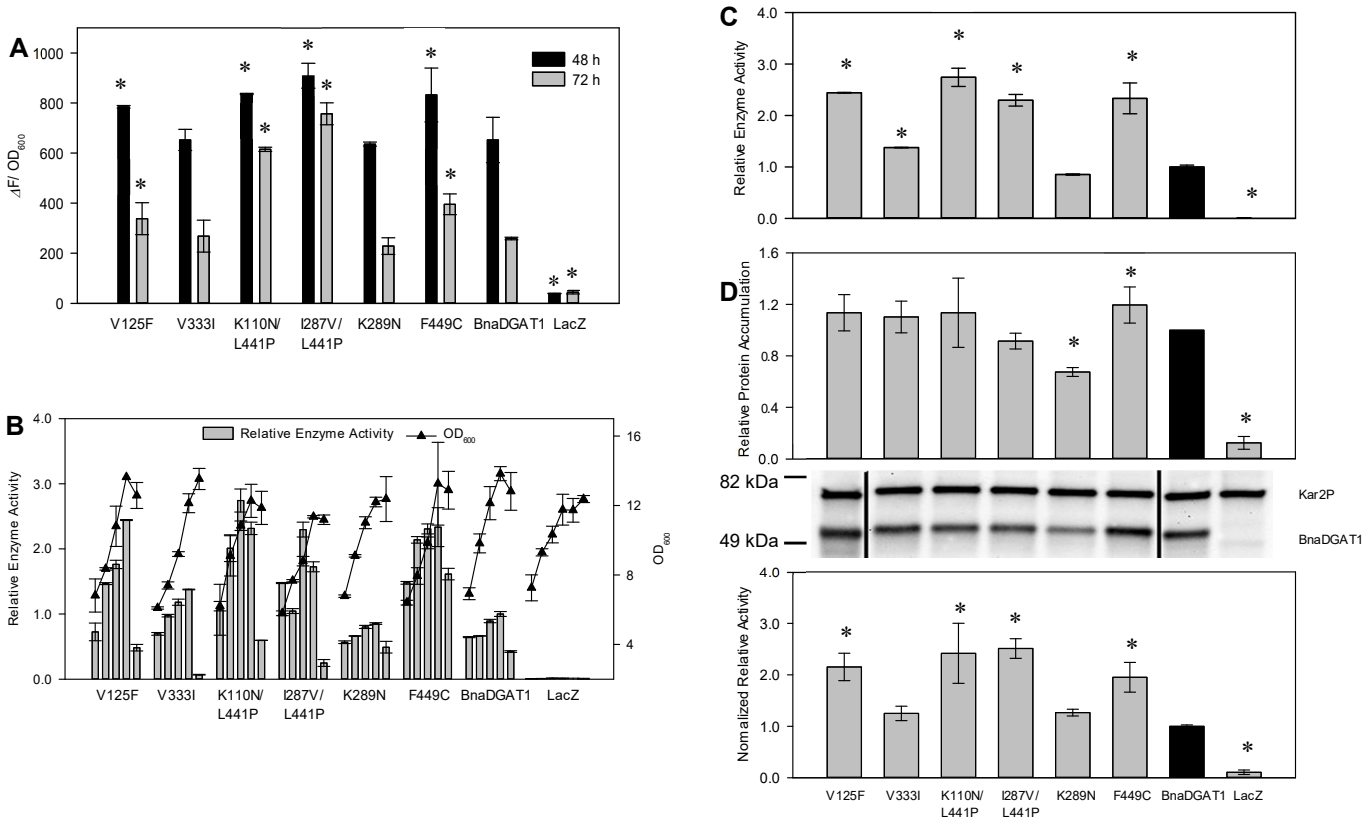

Figure 1. Characterization of BnaDGAT1 variants.

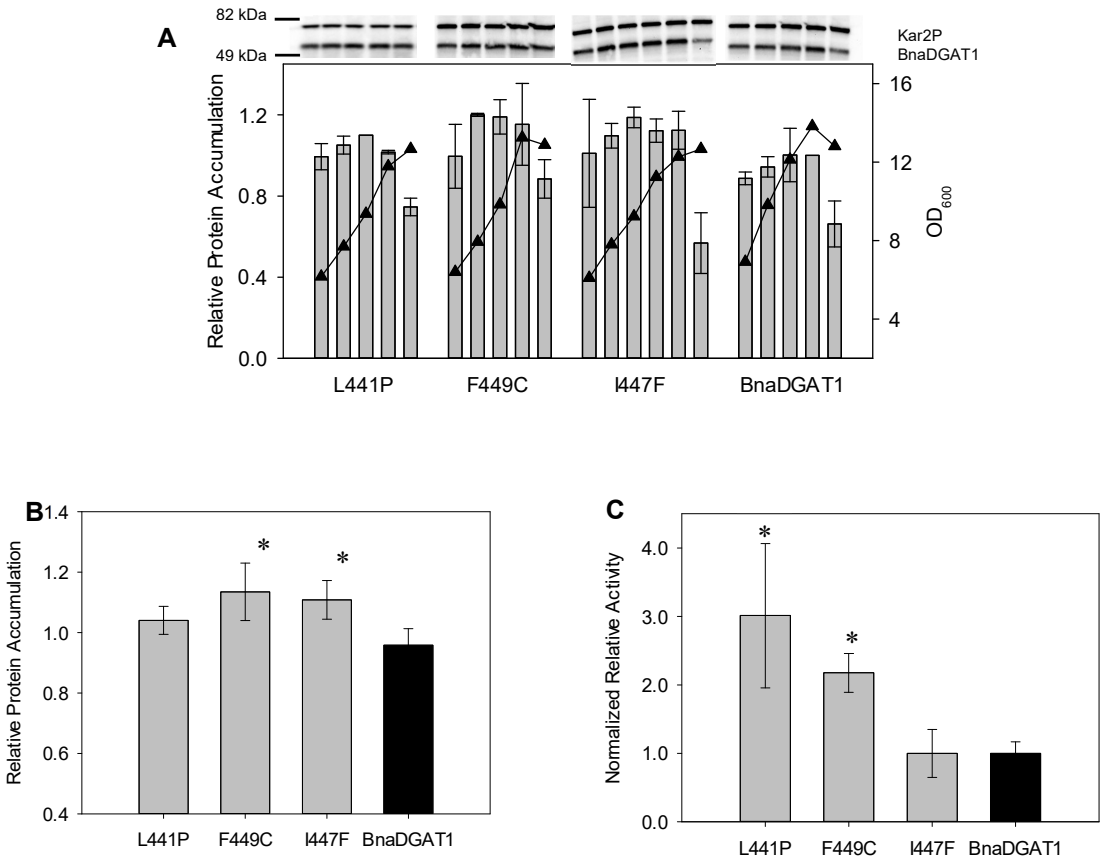

Figure 2. Impact of amino acid residue substitutions in the 9th predicted transmembrane domain of BnaDGAT1 on enzyme activity and accumulation in yeast.

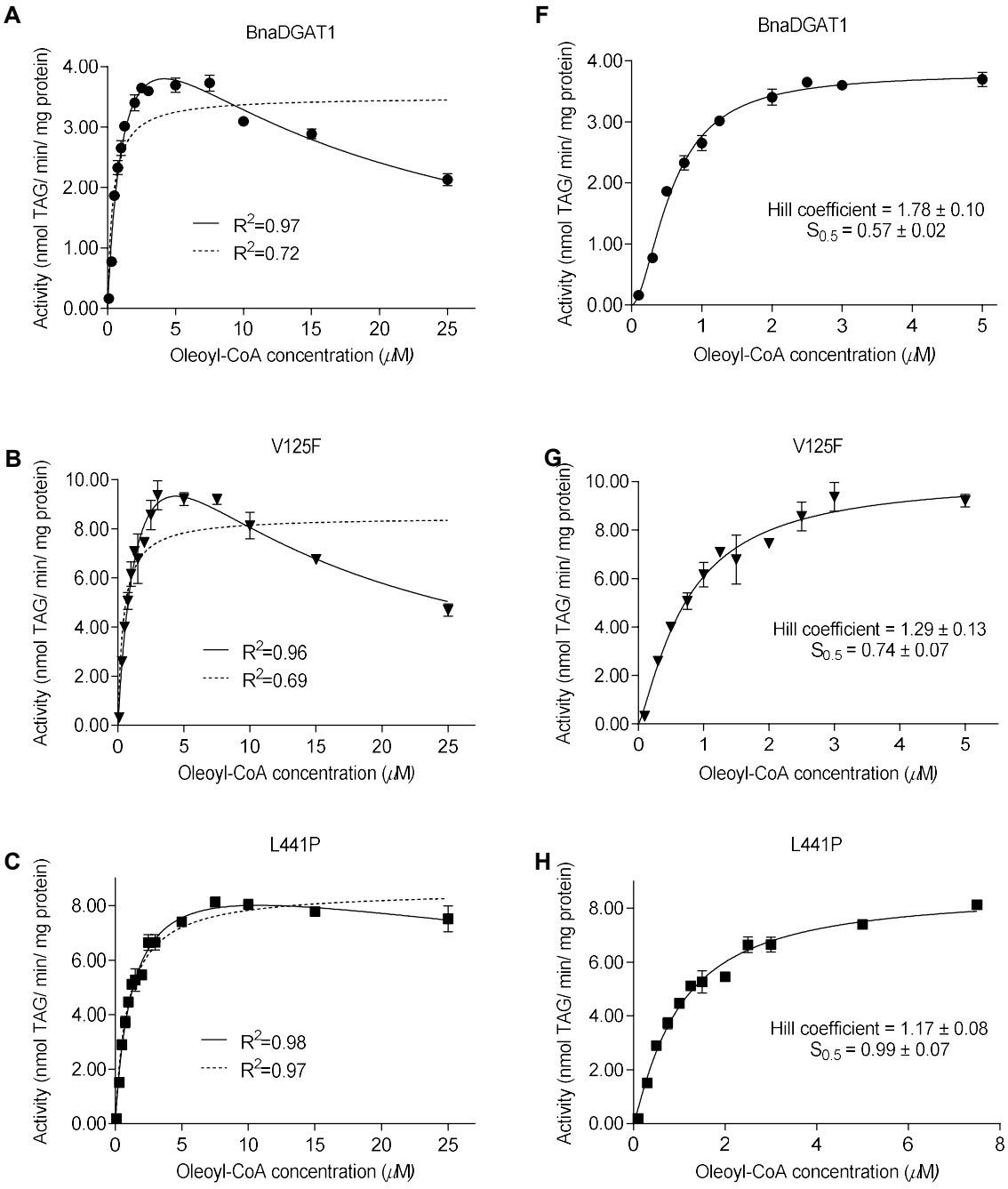

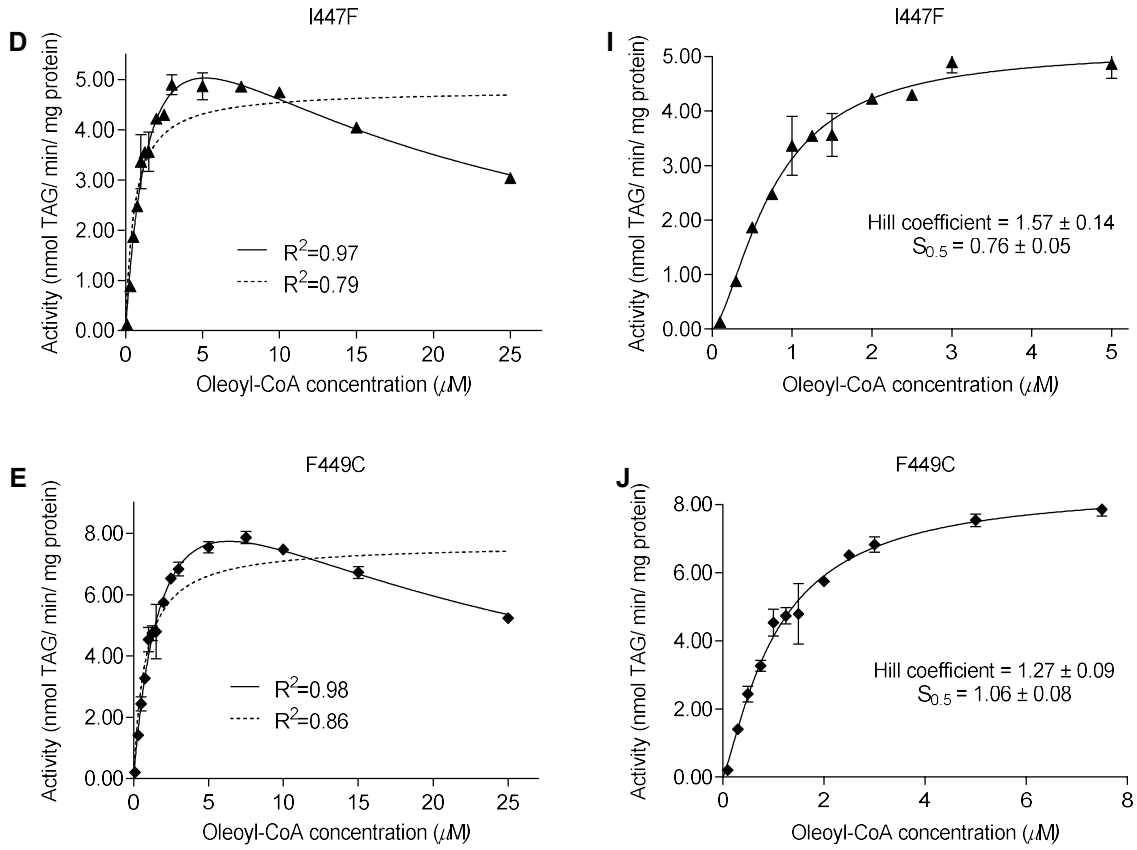

Figure 3. Microsomal DGAT activities of BnaDGAT1 variants at increasing oleoyl-CoA concentrations.

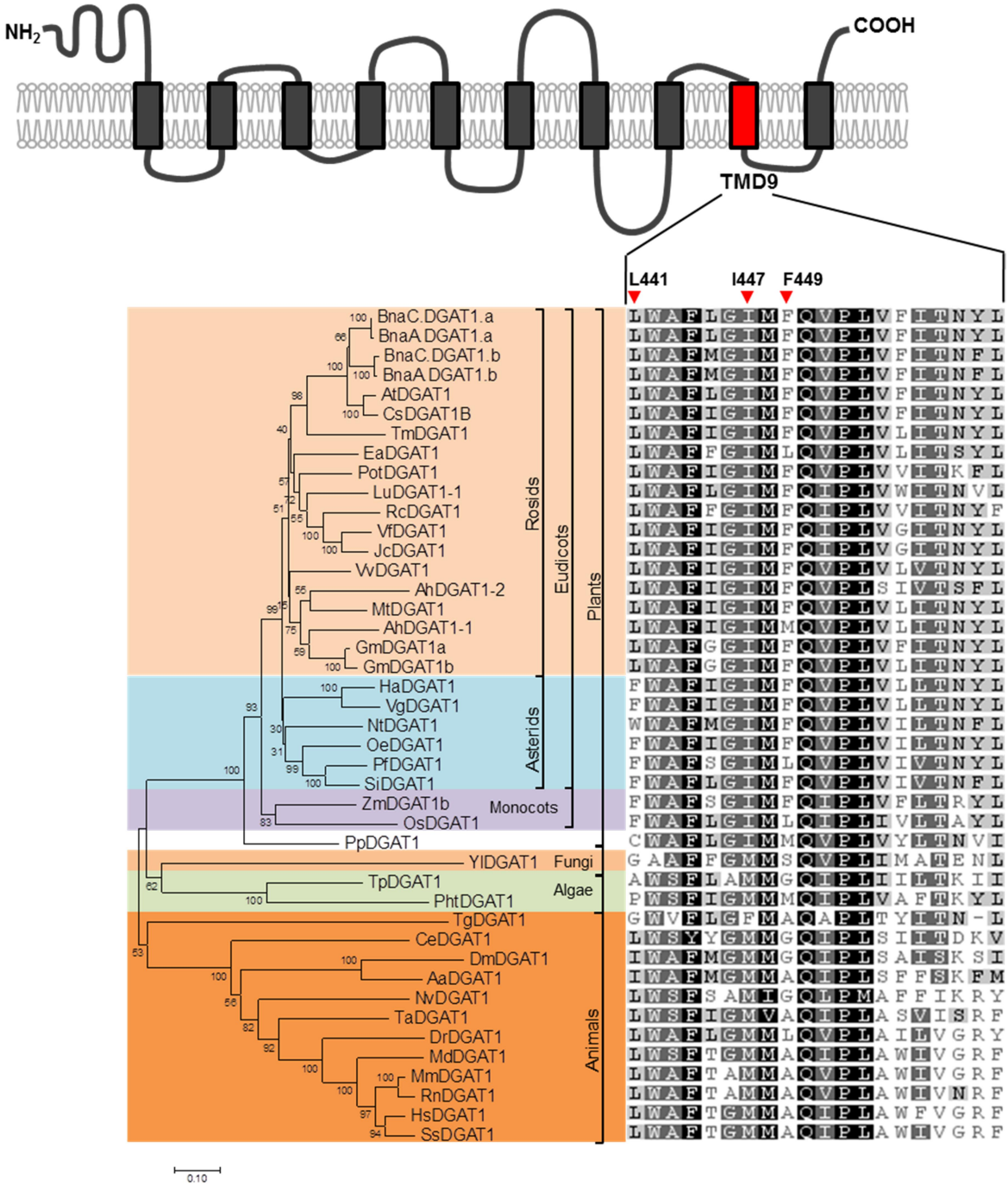

Figure 4. Amino acid sequence analysis of DGAT1 proteins from different species.

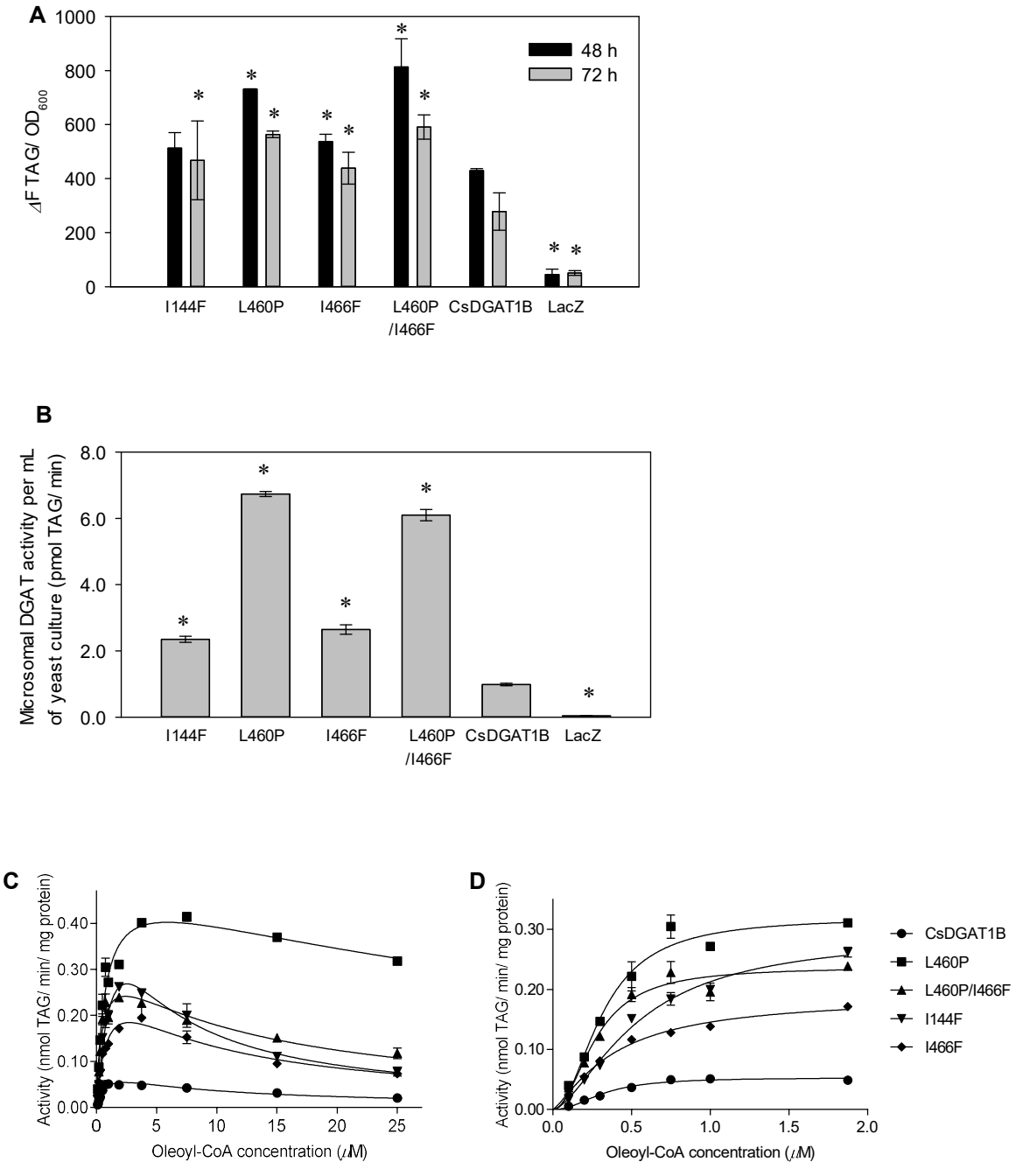

Figure 5. Characterization of CsDGAT1B variants.

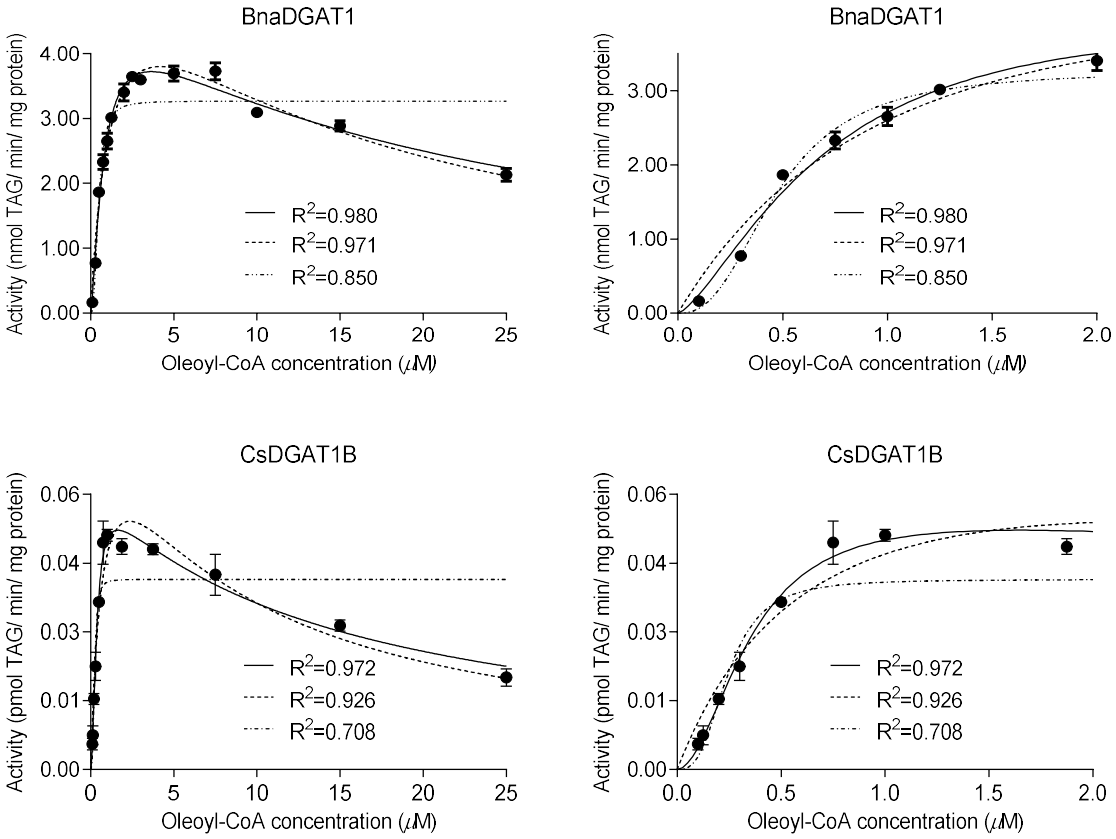

Figure 6. The kinetics of BnaDGAT1 and CsDGAT1B with increasing oleoyl-CoA concentration exhibit a better fit in a kinetic model which accounts for sigmoidicity and substrate inhibition.

Multiple mechanisms contribute to increased neutral lipid accumulation in yeast producing recombinant variants of plant diacylglycerol acyltransferase 1

Yang Xu[1], Guanqun Chen[1], Michael S. Greer[1], Kristian Mark. P. Caldo[1,2], Geetha Ramakrishnan[1], Saleh Shah[1], Limin Wu[3], M. Joanne Lemieux[2], Jocelyn Ozga[1], and Randall J. Weselake[1*]

Appendix A. Supplementary material

Supplementary Table S1. Apparent kinetic parameters of BnaDGAT1 and CsDGAT1B variants obtained from a kinetic model which accounts for sigmoidicity and substrate inhibition. Analysis was performed with GraphPad Prism software using the non-linear regression of the proposed kinetic model (Equation 3). Data are means ± S.D, n = 2 to 3. ND, Not determined.

Supplementary Table S2. Forty-three DGAT1s from different species used for multiple sequence alignment.

Supplementary Figure S1. Initial characterization of BnaDGAT1 variants. A. Analysis of enzyme activity and protein accumulation. Yeast strain H1246 producing recombinant variant enzymes were harvested during the log or stationary phase and then used to prepare microsomes for analysis of *in vitro* DGAT activity, and polypeptide quantification by Western blotting. Each circle represents one BnaDGAT1 variant. Neutral lipid content of yeast expressing corresponding variants was determined by the Nile Red assay and indicated by the size of circle. The relative activity and protein accumulation of wild type (WT) BnaDGAT1 were set as 1.0. B. Production profile of recombinant WT BnaDGAT1 in yeast H1246. Growth rate (optical density, OD_{600}), neutral lipid content (change in fluorescence, ΔF, in arbitrary units) and microsomal DGAT activities of yeast cultures producing BnaDGAT1 are shown. The highest microsomal activity (at 38.5 h) of recombinant WT BnaDGAT1 was set as 1.0. Data are means ± range, n = 2.

Supplementary Figure S2. *In vitro* enzyme activities of BnaDGAT1 variants. Microsomes from yeasts producing recombinant BnaDGAT1 variants were collected at different time points after induction and used for the DGAT assay. The highest microsomal activity of recombinant wild type (WT) BnaDGAT1 was set as 1.0. Growth curve was constructed by measuring OD_{600}. Data are means ± range, n = 2.

Supplementary Figure S3. Copy number (A) and gene expression level (B) of *BnaDGAT* variants in yeast H1246. Data are means ± S.D, n = 3 biological replicates.

Supplementary Figure S4. Alignment of deduced amino acid sequences of *DGAT1* cDNAs from *B. napus* and *C. sativa*. The highlighted amino acid residues indicate the amino acid residue substitutions of BnaDGAT1 variants and the corresponding CsDGAT1B variants.

Table S1 Apparent kinetic parameters of BnaDGAT1 and CsDGAT1B variants obtained from a kinetic model which accounts for sigmoidicity and substrate inhibition. Analysis was performed with GraphPad Prism software using the non-linear regression of the proposed kinetic model (Equation 3). Data are means ± S.D, n = 2 to 3. ND, Not determined.

	$V_{max}{}^{app}$ (nmol/min/mg)	$K_m{}^{app}$ (μM)	$K_i{}^{app}$ (μM)	Hill coefficient	DGAT protein abundance in microsomes (relative to BnaDGAT 1)	$V_{max}{}'{}^{app}$ adjusted for protein abundance (nmol/min/mg)	$V_{max}{}'{}^{app}$ / $K_m{}^{app}$ (mL/min/mg)	$V_{max}{}'{}^{app}$ / $K_m{}^{app}$ relative	R^2
BnaDGAT1 variants									
BnaDGAT1	4.77 ± 0.22	0.79 ± 0.06	22.34 ± 2.92	1.40 ± 0.11	1.00	4.77	6.04	1.00	0.98
V125F	18.95 ± 3.90	2.26 ± 0.96	9.20 ± 2.86	0.92 ± 0.11	1.14	16.69	7.39	1.32	0.96
L441P	9.13 ± 0.45	1.09 ± 0.11	138.80 ± 52.53	1.13 ± 0.08	1.02	8.98	8.24	1.47	0.98
I447F	6.93 ± 0.55	1.19 ± 0.17	22.02 ± 4.24	1.23 ± 0.11	1.12	6.17	5.18	0.93	0.97
F449C	12.84 ± 1.48	2.13 ± 0.48	19.01 ± 4.22	1.02 ± 0.08	1.15	11.13	5.23	0.93	0.98
CsDGAT1B variants									
CsDGAT1B	0.06 ± 0.00	0.37 ± 0.03	14.53 ± 1.84	1.89 ± 0.16	ND	ND	ND	ND	0.97
I144F	0.48 ± 0.08	1.04 ± 0.27	5.06 ± 1.28	1.27 ± 0.14	ND	ND	ND	ND	0.98
L460P	0.46 ± 0.04	0.59 ± 0.12	63.49 ± 26.44	1.14 ± 0.17	ND	ND	ND	ND	0.96
I466F	0.47 ± 0.16	2.34 ± 1.82	4.47 ± 1.98	0.80 ± 0.11	ND	ND	ND	ND	0.97
L460P/I466F	0.26 ± 0.01	0.31 ± 0.03	20.52 ± 4.00	1.81 ± 0.26	ND	ND	ND	ND	0.95

Table S2. Forty-three DGAT1s from different species used for multiple sequence alignment.

Gene	GenBank accession number	Organism
AaDGAT1	XM_001658249	*Aedes aegypti*
AhDGAT1-1	KC736068	*Arachis hypogaea*
AhDGAT1-2	KC736069	*Arachis hypogaea*
AtDGAT1	NM_127503	*Arabidopsis thaliana*
BnaA.DGAT1.a	JN224474	*Brassica napus*
BnaA.DGAT1.b	JN224475	*Brassica napus*
BnaC.DGAT1.a	AF251794	*Brassica napus*
BnaC.DGAT1.b	JN224476	*Brassica napus*
CeDGAT1	NM_001269372	*Caenorhabditis elegans*
CsDGAT1B	XM_010417066	*Camelina sativa*
DmDGAT1	AF468649	*Drosophila melanogaster*
DrDGAT1	NM_199730	*Danio rerio*
EaDGAT1	AY751297	*Euonymus alatus*
GmDGAT1a	AY496439	*Glycine max*
GmDGAT1b	AB257590	*Glycine max*
HaDGAT1	HM015632	*Helianthus annuus*
HsDGAT1	NM_012079	*Homo sapiens*
JcDGAT1	DQ278448	*Jatropha curcas*
LuDGAT1-1	KC485337	*Linum usitatissimum*
MdDGAT1	XM_007488766	*Monodelphis domestica*
MmDGAT1	AF078752	*Mus musculus*
MtDGAT1	XM_003595183	*Medicago truncatula*
NtDGAT1	AF129003	*Nicotiana tabacum*
NvDGAT1	XM_001639301	*Nematostella vectensis*

OeDGAT1	AY445635	*Olea europae*
OsDGAT1	NM_001061404	*Oryza sativa*
PfDGAT1	AF298815	*Perilla frutescens*
PhtDGAT1	HQ589265	*Phaeodactylum tricornutum*
PotDGAT1	XM_006371934	*Populus trichocarpa*
PpDGAT1	XM_001770877	*Physcomitrella patens*
RcDGAT1	XM_002514086	*Ricinus communis*
RnDGAT1	AB062759	*Rattus norvegicus*
SiDGAT1	JF499689	*Sesamum indicum*
SsDGAT1	NM_214051	*Sus scrofa*
TaDGAT1	XM_002111989	*Trichoplax adhaerens*
TgDGAT1	AY327327	*Toxoplasma gondii*
TmDGAT1	AY084052	*Tropaeolum majus*
TpDGAT1	XM_002287179	*Thalassiosira pseudonana*
VfDGAT1	DQ356680	*Vernicia fordii*
VgDGAT1	EF653276	*Vernonia galamensis*
VvDGAT1	AM433916; CAN80418	*Vitis vinifera*
YlDGAT1	XM_502557	*Yarrowia lipolytica*
ZmDGAT1b	EU039830	*Zea mays*

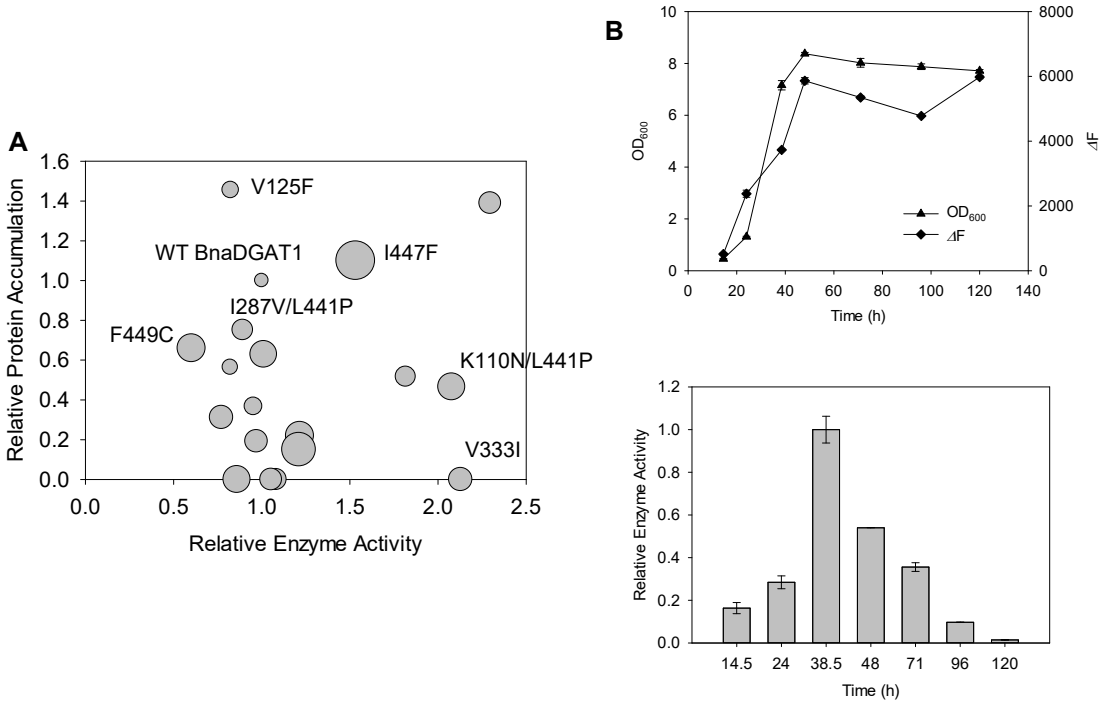

Figure S1. Initial characterization of BnaDGAT1 variants.

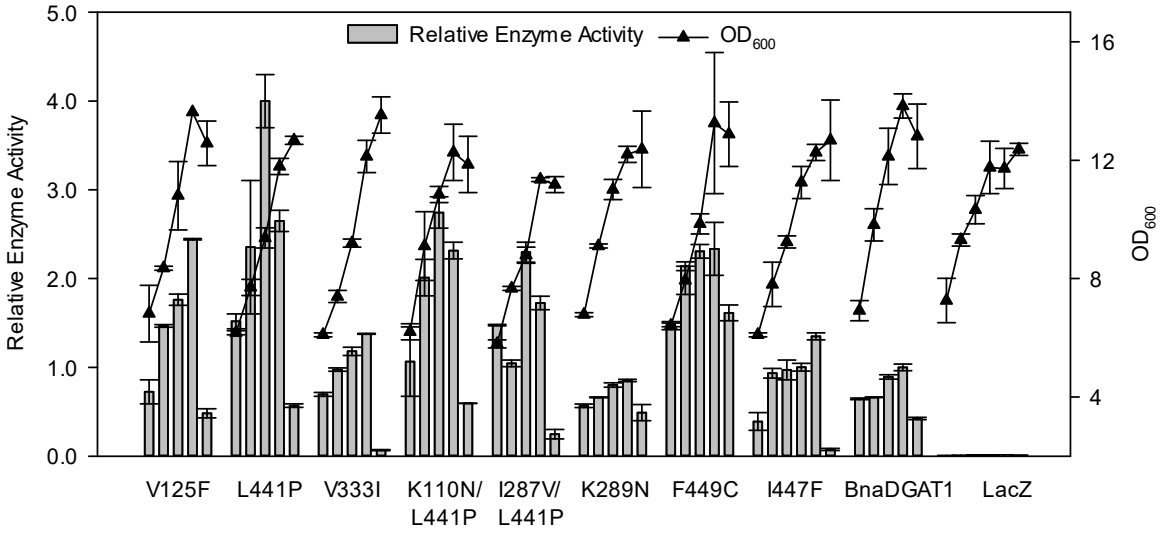

Figure S2. *In vitro* enzyme activities of BnaDGAT1 variants.

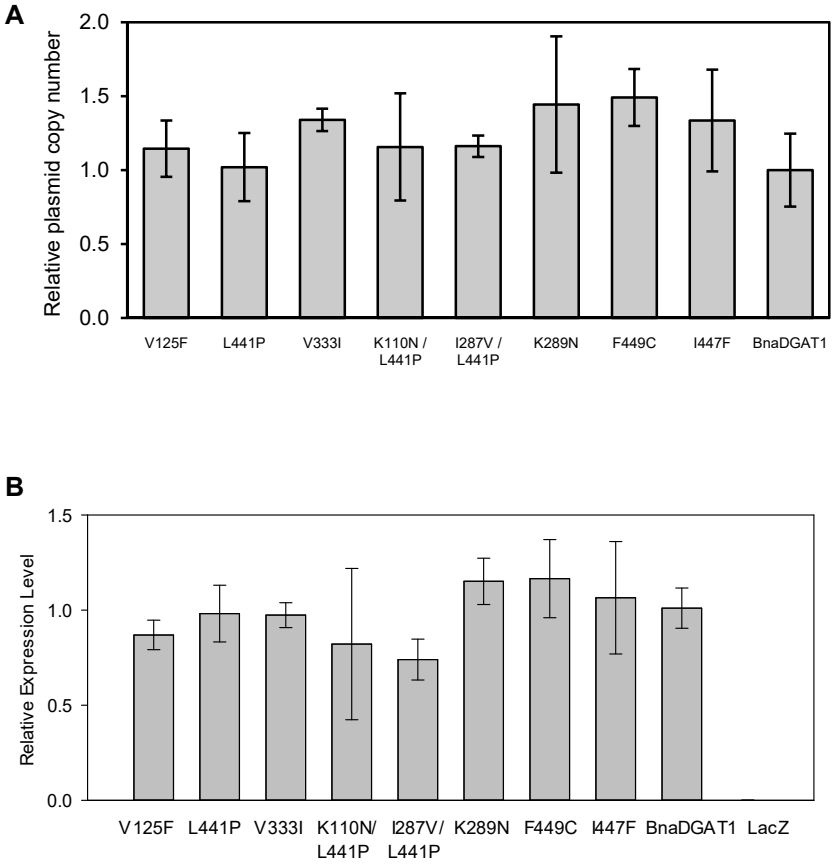

Figure S3. Copy number (A) and gene expression level (B) of *BnaDGAT1* variants in yeast H1246.

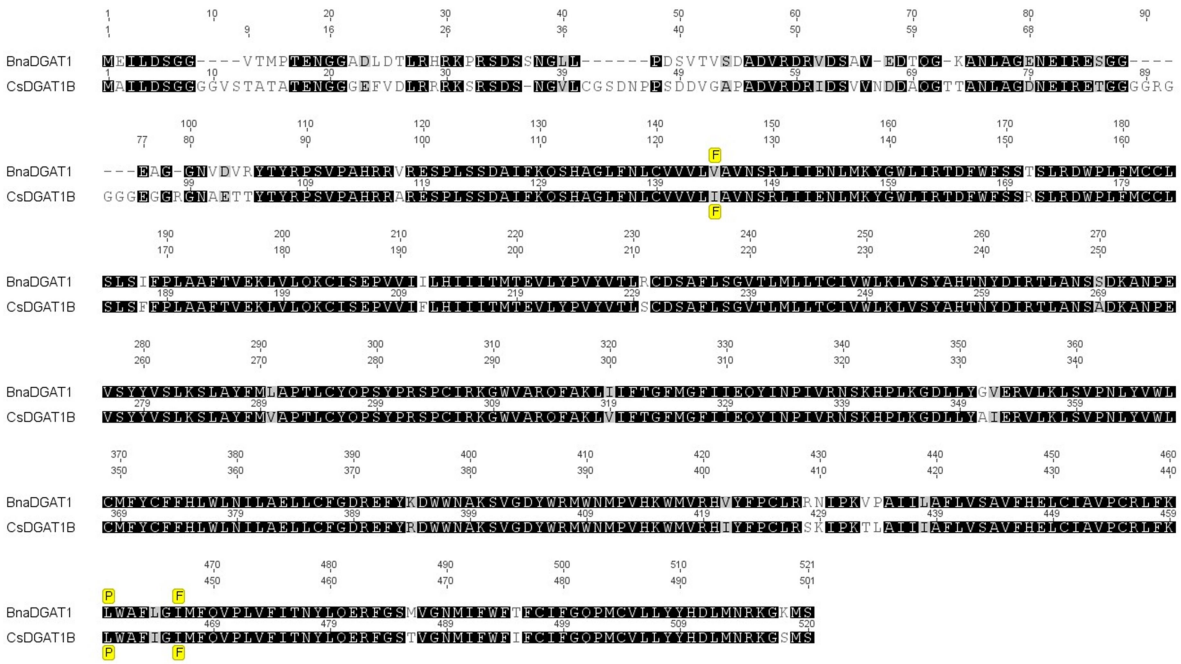

Figure S4. Alignment of deduced amino acid sequences of *DGAT1* cDNAs from *B. napus* and *C. sativa*.